SYNTHESIS AND CHARACTERIZATION OF ELECTROCERAMIC FOAMS FOR 3-3 PIEZOELECTRIC COMPOSITES

By

LAUREL WUCHERER

A THESIS PRESENTED TO THE GRADUATE SCHOOL
OF THE UNIVERSITY OF FLORIDA IN PARTIAL FULFILLMENT
OF THE REQUIREMENTS FOR THE DEGREE OF
MASTER OF SCIENCE

UNIVERSITY OF FLORIDA

2008

ACKNOWLEDGMENTS

First of all, I would like to acknowledge my advisor, Dr. Juan C. Nino, for his support and guidance. His high standards and constant encouragement to strive for the best led me to many opportunities during my college career and for my future professional career. I thank Dr. Ghatu Subhash for his invaluable suggestions and rewarding discussions. I would also like to thank my other committee members (Dr. Wolfgang Sigmund and Dr. Jacob Jones) for their time. Further, I would like to thank Professor Enrico Traversa and Francesco Basoli for their innovative work in the field of ceramic foams which gave me the motivation and fundamentals to begin my research.

I would also like to convey my heartfelt thanks to the former and current group members of NRG (Nino Research Group): Samantha Yates, Shobit Omar, Lu Cai, Wei Qiu, Peng Xu, Mohammed Elshennawy, Satyajit Phadke, Marta Giachino, Kevin Tierney, Donald Moore, Kevin Lee, Louis Perez, Julian Gomez and Adam Wilk for providing me with an excellent research environment and helpful advice.

I also wish to acknowledge all of my friends at the University of Florida (UF) with whom I experienced ALL of Gainesville during the last 4-and-half years. Without Nikki and Kristen, the triumvirate would not have prevailed. I am especially grateful to UF's Danza Dance Company which gave me the creative outlet to pursue my passion of dance during my college years. Final "cheers" go to my former roommate, Michelle Motola, who endured my long hours and mood swings during the hard times.

Finally, I am grateful to my entire family, especially my mother Pat Poole, my father Carl Wucherer and my "mini-me" Devon, who provided me with the intelligence and confidence to take advantage of all life has to offer.

TABLE OF CONTENTS

page

LIST OF TABLES

LIST OF FIGURES

Abstract of Thesis Presented to the Graduate School
Of the University of Florida in Partial Fulfillment of the
Requirements for the Degree of Master of Science

SYNTHESIS AND CHARACTERIZATION OF ELECTROCERAMIC FOAMS FOR 3-3 PIEZOCOMPOSITES

By

Laurel Wucherer

December 2008

Chair: Juan C. Nino
Major: Materials Science and Engineering

We investigated processing-structure-property-performance interrelationships of barium titanate foam in 3-3 piezocomposites for sensor applications. The first area of investigation focuses on the tailoring of the foam microstructure via processing parameters. Barium titanate foams were synthesized via direct foaming method using commercial powders. In order to control the microstructure and by extension the properties, synthesis parameters such as foaming agent, composition, sintering time, and sintering temperature were varied to determine their influence. Microstructure was classified in terms of strut characteristics, average grain size, average cell window size, porosity, and grain boundary integrity. The two systems that fabricated homogeneous structures favorable to ultrasonic sonar applications were a laboratory developed and a commercial polyurethane system, both silicon-free. When sintered at 1400 degrees Celsius for 8 hours they produced thick, dense struts and uniform cell window-size distributions, though with different characteristics. The foam prepared with the laboratory synthesized polyurethane had a porosity of 90 percent, an average grain size of 44 microns, and an average cell window size of 67 microns, while the foam prepared with the commercial polyurethane had a porosity of 87 percent, an average grain size of 20 microns, and an average cell window size of 99 microns.

The second area of investigation was the resulting mechanical properties of the foams. They were measured using confined compression testing to determine if the foams had acceptable properties for their intended application and could withstand handling. The mechanical properties (compressive modulus and collapse stress) determined from the experimental data increased with increasing density. Additionally, the lab developed PU foam showed a higher mechanical strength due to a higher average density. The data was then fit with a phenomenological model. The focus of this work is on the elastic response due to the application requirements.

The final area of investigation is the infiltration of the foam with polymer to create a 3-3 piezocomposite. Polymer selection was based on a criterion of material properties including viscosity, cure time, cure temperature, and hardness. The samples were infiltrated with Epofix epoxy using Epovac infiltration equipment which is a vacuum impregnation system that infiltrates all empty space in the foam created by the cell window network with the epoxy. Using SEM, it was determined that the foam was completely infiltrated, creating a 3-3 composite.

Preliminary electrical characterization of the piezoelectric properties indicated that the hydrostatic figure of merit of the composite was calculated to be lower than that of bulk barium titanate and bulk lead zirconate titanate. This is due to the low compliance of the polymer chosen for the composite and the lower piezoelectric properties of barium titanate in comparison to PZT and the low volume fraction of piezoelectric material in the composite. Based on these results, the next step is to create a 3-3 composite with lead zirconate titanate to determine if the piezoelectric properties are further enhanced in this system. From the areas investigated above, it is concluded that the 3-3 piezoelectric composite is achievable.

CHAPTER 1
INTRODUCTION

1.1 Statement of Problem and Motivation

Foams, specifically ceramic-based, offer unique and favorable properties, but their use has been limited by the inability to predict and control the resulting microstructure during processing, especially using a direct foaming method since the process relies on the incorporation of gas bubbles to create the foam. By establishing process-microstructure-property interrelationships, the microstructure of the foams, and inherently the properties, can be tailored for many different applications.

The purpose of this work is to explore the electroceramic properties of $BaTiO_3$ foam for electromechanical applications. The intent is to use $BaTiO_3$ as a test material and eventually, create piezoelectric composites based on materials such as PZT and piezoelectric polymers. This piezocomposite could be used in sonar and ultrasound application by creating an open-cell structure that has the potential to exhibit 3-3 connectivity by creating a three-dimensional network of cell windows and ceramic struts. Therefore the investigation of the synthesis of $BaTiO_3$ foams using the direct foaming method and ceramic powder precursor for engineering of piezocomposites is of significant interest.

1.2 Scientific Approach

The literature review can be briefly summarized as follows: Newnham et al.[1] published a pioneering work in the area of piezoelectric-polymer composites, which included the composite connectivity notation currently used and internationally accepted. This notation is further discussed in Chapter 3. One of the most common types of composites fabricated due to its increased enhancements of piezoelectric property and successful processing is the 1-3 composite made from piezoelectric rods in a passive polymer matrix whose key engineering aspects for design have been identified through extensive experimental and theoretical work led primarily by Haun et al.[2,3] and by Smith et al.[4,5,6,7]. However, Skinner et al.[8], was the first to

report piezocomposites with 3-3 connectivity using a lost-wax method with coral as the starting material. Other sacrificial methods were investigated by Shrout et al.[9] and Rittenmyer et al.[10] From this work, it was discovered that larger piezoelectric coefficients were obtained using soft polymer as the second phase because its higher elastic compliance promoted stress transfer to the ceramics, which is highlighted in the hydrostatic figure of merit, discussed in Chapter 2.

In the field of ceramic foams, the first major break though was the patent by Schwartzwalter et al.[11] for polymer foam replication method 40 years ago. Since then, the research has expanded to incorporate many different processing methods, which have been reviewed by Gauckler et al.[12], and many different ceramics including open-cell and closed-cell SiOC foams by Colombo et al.[13], cordierite foams by Costa Oliviera et al.[14], and open-cell Al_2O_3 foams by Peng et al.[15]

After careful review of the literature, it is clear that ceramic foams and piezocomposites have been studied in the past but even though areas such as microstructure, processing and properties have been investigated individually, very little has been done to understand the interrelationships between these individual areas. Specifically electroceramic foams have not been thoroughly investigated to realize their potential to fabricate 3-3 composites for piezoelectric sensors. Therefore, the scientific objective of this thesis is to fabricate foamed piezoelectric ceramic-polymer composites with 3-3 connectivity and controlled microstructure, and to investigate the effect that a tailored ceramic microstructure has on the electromechanical properties of the composite.

In order to accomplish this, further investigation in areas such as processing, microstructural optimization, mechanical property characterization, polymer infiltration and electrical property characterization is required.

In processing for example, very little is known about the influence of variation in processing parameters on the final microstructure, or the reproducibility of the structure using direct foaming method since gas incorporation is not easy to control. While there are previous

publications on the design requirements of 1-3 composites, there is insufficient work on the design requirements of 3-3 composites and for piezoelectric sonar sensors, specifically an optimal microstructure for both. Experiments regarding these issues will be conducted.

Once an optimum foam microstructure is fabricated, it is necessary to evaluate the reproducibility and standardization of the process; therefore, multiple foamed samples from the same mixture batch will be fabricated and characterized to assess the sample to sample variation. Additionally, the mechanical properties of the foam will be measured using confined compression testing and fitted using a phenomenological model established by Subhash et al.[16] specifically for the mechanical behavior of foams.

After determining the ideal precursors and processing conditions for synthesizing the foams, polymer will be infiltrated into the ceramic foam skeleton to create a 3-3 composite. Special attention will be given to polymer selection as it will determine the magnitude of piezoelectric property enhancement. A common vacuum and pressure assisted technique will be employed to achieve the complete infiltration of the ceramic foam.[17,18] Once a 3-3 composite has been achieved, the electrical properties will be measured including dielectric, ferroelectric and piezoelectric characterization. A hydrostatic figure of merit (HFOM) of the piezocomposite will be determined and compared to the HFOM of other piezocomposites and piezoelectric materials.

CHAPTER 2
BACKGROUND

The present chapter presents a brief summary of some of the theoretical background required for understanding and analyzing the investigation presented in the subsequent chapters. As a summary, it is not intended to cover the background of the research areas in their entirety, but rather to present a work frame for the rest of the thesis.

2.1 Piezoelectricity

Piezoelectricity can be defined as the linear coupling between mechanical stress, *X*, and electric polarization, *P* (referred to as direct effect) or as the coupling of mechanical strain, *x*, and applied electric field, *E* (converse effect). Piezoelectricity is a third-rank tensor property since it relates the polarization vector, *P*, to stress, *X*, a second-rank tensor. Tensor notation set aside, the principal piezoelectric coefficient, *d*, describes the direct effect as well as the converse effect. This implies that the units of *d* are [C/N] or [m/V]. Typical values for useful piezoelectric materials range from ~ 2 pC/N (α-quartz) to ~ 800 pC/N (lead zirconate titanate, PZT ceramics). The converse piezoelectric effect of material is useful for actuation applications, while the direct piezoelectric effect can be exploited in sensing applications, directly related to this work. Naturally occurring piezoelectric materials include minerals such as tourmaline and quartz. Quartz is widely used in frequency control and time keeping applications. In the area of polycrystalline materials the most important family of piezoelectrics is that of perovskite-based (e.g. $BaTiO_3$, PZT, etc) ceramics. An abbreviated overview of piezoelectric ceramics is discussed in the following section.

2.2 Piezoelectric Ceramics

For over 50 years since the report on the piezoelectric properties of $BaTiO_3$ and PZT, by Roberts[19] and Jaffe et al.[20], respectively, perovskites have been at the forefront of transducer technology. To date, barium titanate ceramics are used in applications as diverse as underwater sonar, biomedical ultrasound, multilayer actuators for fuel injection, bimorph pneumatic valves

and picoliter pumps for inkjet printers. $BaTiO_3$ (Figure 2-1) crystallizes with the perovskite structure.

The larger Ba atoms (red) occupy the corners of the unit cell and establish a twelve-fold coordination with oxygen (blue) which occupies the face centers. Together they form a cubic close-packed arrangement with a typical lattice parameter around 4 Å.[21] Titanium ions (green) occupy the center of the unit cell and establish an octahedral coordination with oxygen. The high temperature form of $BaTiO_3$ is cubic (space group Pm3m) and on cooling a phase transformation occurs in which the atoms are displaced to a tetragonal phase (space group P4mm). $BaTiO_3$ exhibits phase transformations which cause ferroelectric and paraelectric behavior depending on the temperature and structure. It has unique electronic properties including a high dielectric constant (1400), piezoelectricity (d_{33} = 190 pCN^{-1}), ferroelectricity (T_c = 130 °C), and pyroelectricity (p = 20 nC/cm^2 °K). In addition, it exhibits good mechanical strength and a high melting temperature (T_m = 1625 °C).[4] Typical piezoelectric coefficients for other polycrystalline ceramics are shown in Table 2-1.

2.3 Ceramic-Polymer Piezoelectric Composites

In general, the aim of composite technology is to combine materials in such a way that the composite exhibits optimum properties and performance far exceeding the behavior of each of its individual members. Based on the work by Newnham et al.[1] (Chapter 1) using a simple cube model, two-phase composites were labeled by a two number notation, the first defining how the ceramic phase is connected in space and the second number indicating how the polymer is connected. There are ten connectivity patterns in a two-phase composite, ranging from a 0-0 unconnected checkerboard pattern to a 3-3 pattern in which both phases are three dimensionally self-connected. Some of the images from the now legendary figure from Newnham's work are reproduced in Figure 2-2. From these configurations, by far the most widely used for sonar, medical imaging and non-destructive testing applications is the 1-3 type composites made from piezoelectric rods in a passive polymer matrix.

Of particular interest and direct relevance to this work, however, is the previous work on 3-3 piezoelectric composites. Expanding on the literature review in Chapter 1, Shrout et al.[8] developed a simplified fabrication process involving the burn-out of polymer spheres referred to as BURPS (BURned-out Plastic Spheres). Using this method with polymethyl methacrylate as the sacrificial polymer, Rittenmyer et al.[10] sintered porous PZT skeletons and later impregnated them with a stiff vinylcychlohexane dioxide epoxy and a soft silicone elastomer. It was found that the larger piezoelectric coefficients were obtained for the softer polymer because its higher elastic compliance promotes stress transfer to the ceramic. It was found that the hydrostatic figure of merit (HFOM) for hydrophone applications $d_h g_h$ was more than a hundred times than that of PZT ceramics. HFOM is defined as

$$HFOM = d_h g_h \quad (2\text{-}1)$$

$$d_h = d_{33} + 2d_{31} \quad (2\text{-}2)$$

$$g_h = \frac{d_h}{\varepsilon_{33}^T} \quad (2\text{-}3)$$

Figure 2-3 shows the difference in HFOM between different piezocomposites reviewed by Cross[22]. Besides the hydrostatic sensitivity, additional advantages of these composites include low dielectric constant, high compliance, mechanical flexibility and low density which will enable improved matching of acoustic impedance to water (1.569 MRayls)[4].

A summary of the dielectric and piezoelectric properties of 3-3 type composites is shown in Table 2-2 after Gururaja et al.[23] It has to be said that the figure of merit of these composites, although high, are at least an order of magnitude below other composite configurations such as diced PZT polymer composite (20,000 x 10^{-15} m^2/N); however this process is complicated and relies heavily on the minimization of the feature sizes (< 100 μm). Therefore the ability to increase the figure of merit while maintaining a simple processing method is desired.

The 3-3 piezocomposite is engineered by infiltrating the cell window network completely with polymer so that each component has 3-dimensional connectivity. Composites with 3-3 connectivity are desired because they offer a higher piezoelectric enhancement.

2.4 Ceramic Foams

In the past, metallic and polymeric foams have commonly been used in industry due to high mechanical strength and ductility, respectively. However, porous ceramics have become more interesting in an industrial sense because they have low density, low thermal conductivity, high specific strength, high thermal shock resistance, and high surface area.[24] Depending on their structure, ceramic foams can be used in corrosive filtration systems, thermal insulation, acoustic receiving systems, scaffolds for bone tissue engineering and solid oxide fuel cells.[25]

The growing scientific and industrial interest is the result of the properties of this material form such as low thermal conductivity, low dielectric constant, low density, high permeability, etc. In addition, the incorporation of fillers allows for the fabrication of structures with tailored thermal, electrical, magnetic, and mechanical properties.[24] Technically speaking, ceramic foams are a specific class of porous materials that consists of a three-dimensional array of polyhedral cells and a total porosity greater than 45 vol%.[26] The cells can be surrounded by ceramic walls and struts (defined in next section), a 3-D interconnected structure is formed with open porosity and the material is referred to as open-cell foam. As such, open-cell foams can be considered as 3-3 composites between ceramic and air, and as the backbone for 3-3 ceramic composites in general. They are, therefore, a key component of this work.

Remarkably, despite the enormous success and recent progress in ceramic foam science and technology, there has been no systematic study regarding the control of the ceramic microstructure. In general, research that has dealt with structural control has focused on the control of the cell and strut configuration, or the foam mesostructure. While a controlled mesostructure is essential to the mechanical integrity and connectivity of the foam, the microstructure (i.e. grain size, grain boundary configuration, etc) plays an essential role in the general properties of the ceramic foam. This is especially important in electroceramics such as piezoelectrics and ferroelectrics where grain size and grain boundary configuration directly

affect, among others, the dielectric permittivity and domain wall mobility, which in turn affects poling and the overall piezoelectric response of the material.

Before continuing it is imperative to clarify the terminology used throughout this thesis to describe the micro- and meso-structure of the foam. There are three major components (Figure 2-4): the ceramic strut, grain and cell window. The ceramic strut consists of a number of grains and is the interconnected ceramic network that will eventually be the ceramic phase of the composite. The cell windows are the interconnected cell window phase, and will eventually be the polymeric phase of the composite. Foam structures with this interconnected cell window network, are considered open-cell foams. Pores in foams, refer to the holes in the struts either in the grains or at the grain boundaries. Cells refer to the hemispherical voids consisting of cell windows and cell walls, which are struts within the cell. The mesostructure is classified in terms of strut, cell walls, cells and cell windows. The microstructure is classified in terms of grain size, grain boundary configuration and porosity. Both must be understood to control the overall structure of the foam. The shape and size of these features are determined by processing parameters. This will be discussed in the next section and more thoroughly in Chapter 3.

2.5 In-Situ Foam Processing

There are three common foaming methods (Figure 2-5): replica, sacrificial template and direct foaming. Replica method (1) is the impregnation of a cellular structure with a ceramic suspension or precursor solution which forms to the morphology of the original cellular structure. While it's a convenient method, it produces low strut stability and limited cell window size due to the limitations of the template. Sacrificial template method (2) is the preparation of a composite consisting of a continuous ceramic matrix and homogeneously dispersed particles which are extracted to produce pores. These foams have a wide range of porosities and higher mechanical strength then that of the replica method. Direct foaming method (3) relies on the stabilization and setting of wet foams (either by surfactant or particles) produced by directly

incorporating air bubbles into a ceramic suspension using a foaming agent such as a polyurethane system. This method eliminates the need to extract a sacrificial phase before sintering and produces the highest mechanical strength of the three methods while still maintaining a wide range of pore sizes and porosities.[12]

Expanding on these three methods, a wide range of processes for the production of ceramic foams have been demonstrated and have been recently reviewed. Perhaps the most widely used method is the sponge replica technique in which a polymer sponge is impregnated with ceramic slurry and followed by burn-out of the polymer and high temperature sintering of the remaining ceramic. Bao et al.[27] have demonstrated a variation of this technique in which a polymer precursor for the ceramic, or preceramic, is used. Recently direct foaming of sol-gel ceramic precursors without the use of sacrificial templates has been reported. These processing techniques have been used to synthesize several ceramic foams including alumina[28], SiOC[13] (Figure 2-6a) and PZT[14]. In the case of SiOC a fine grain size (less than 3 μm) is obtained. A similar structure is seen for the Al_2O_3 foam by Colombo and Hellmann in Figure 2-6c. Further, the detail of the strut in the Al_2O_3 ceramic foam indicates a hollow internal structure (Figure 2-6b). In contrast, the direct foaming process typically leads to open cell structures with small cell windows as seen in Figure 2-6d.

This work utilizes a direct foaming technique that Traversa and collaborators[29] employed and developed to successfully fabricate NiO-YSZ foams for anodes in solid oxide fuel cells. The technique is based on the in-situ polymerization of a polyurethane system (PU) loaded with ceramic powder with the addition of surfactants, followed by a precisely controlled firing schedule. Due to the instable nature of the vapor-liquid interface created during the foaming process, the polyurethane systems are usually created using particles or surfactants to stabilize this interface. However, most commercial systems are surfactant-stabilized systems. The ceramic powder is dispersed separately in the two components of a commercial polyurethane system. The two components are mixed to induce polymerization and the mix is placed in an

open Teflon mold. The chemical reaction of the PU is shown in Figure 2-7. The reaction produces carbon dioxide which form bubbles within the structure and will eventually produce cells or cell windows after sintering.

Figure 2-8 shows a summary of the processing steps for this technique using a PU developed by Traversa et al.[29] at the University of Rome – Tor Vergata. The PU consists of methyl diphenyl diisocyanate (MDI) and polyethylene glycol (PEG)/1, 4-Diazabicyclo-(2.2.2)octane (1,4-Dabco), which constitute the PU. Tween 80 is added as a pore minimizer and water acts as a catalyst.

In addition, a similar method is employed using commercially purchased PU systems rather than lab developed as the once discussed above. The difference between the two systems is the type of diisocyanate and polyol used which determine the resulting microstructure.

Table 2-1. Piezoelectric coefficients of selected ceramics (in pC/N)

Polycrystalline Ceramics	d_{33}	d_{31}	d_{13}	d_{32}	d_{24}
$BaTiO_3$[4]	190	-78	260	-	-
PZT-5H[41]	593	-274	741	-	-
PZT-8[41]	225	-27	330	-	-
$PbNb_2O_6$	60	-43	180	24	170
$Na_{0.5}K_{0.5}NbO_3$	127	-51	306	-	-

Table 2-2. Dielectric and piezoelectric properties of 3-3 composites[23]

Composites	ρ (kg/m^3)	K_{33}	d_{33} (pC/N)	g_{33} (mVm/N)	g_h (mVm/N)	$d_h g_h$ (10^{-15} m^2/N)
Coral Replamine	3300	50	100	225	140	5040
PZT-Spurrs epoxy	4500	620	150	28	20	2200
PZT-silicone rubber	4000	450	200	50	45	8100
Porous PZT	3840	200	190	130	50	4500
Barium titanate	6020	1400	190	-	2.7	93

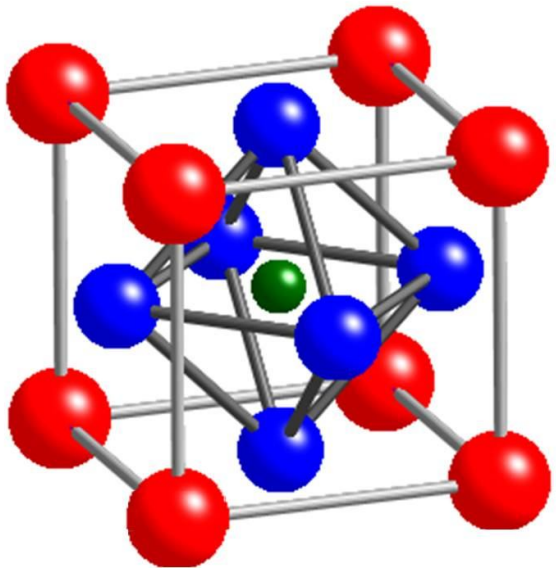

Figure 2-1. Barium titanate unit cell with barium (red), oxygen (blue) and titanium (green) atoms.

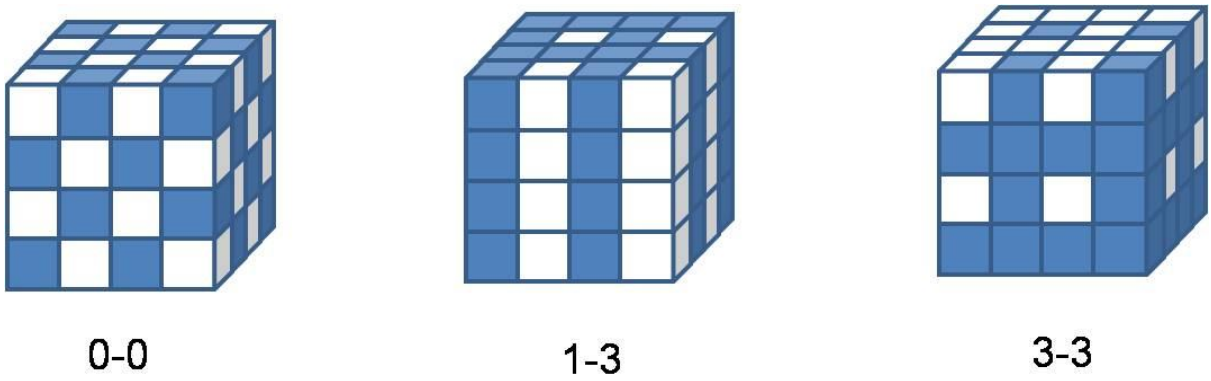

Figure 2-2. Three of the ten connectivity patterns commonly used for composites by Newnham et al.[1]

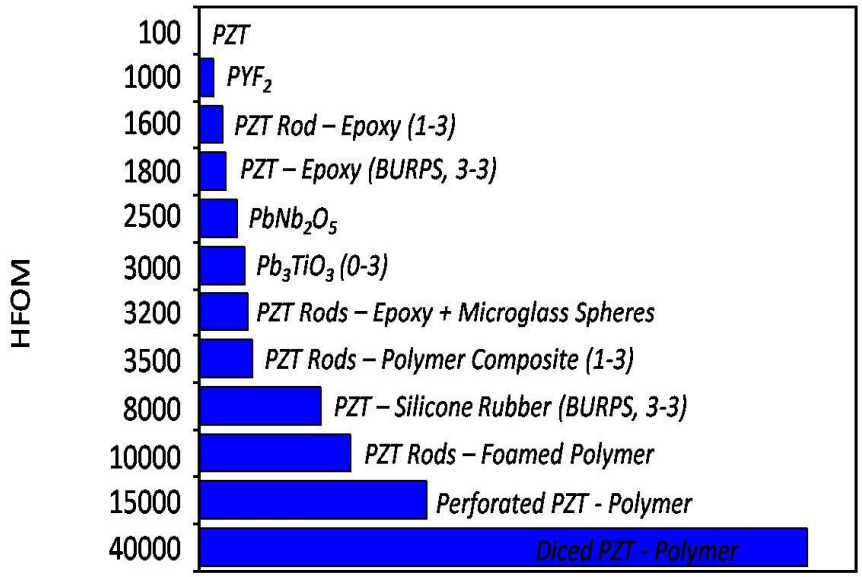

Figure 2-3. Comparison of HFOM for different ceramic-polymer composites.

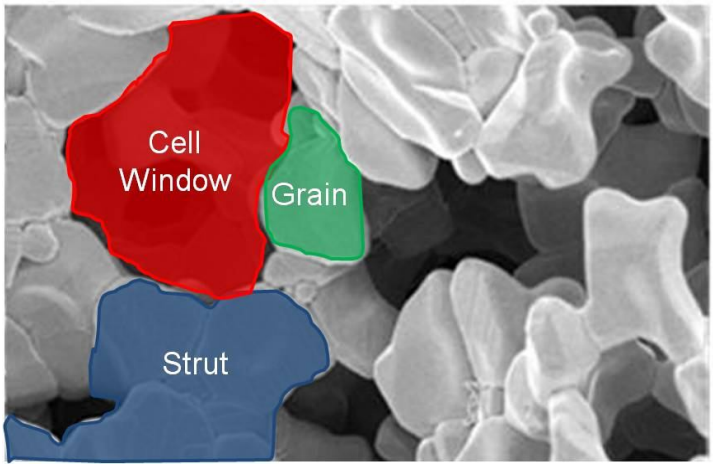

Figure 2-4. Scanning election microscopy image depicting components of the foam microstructure.

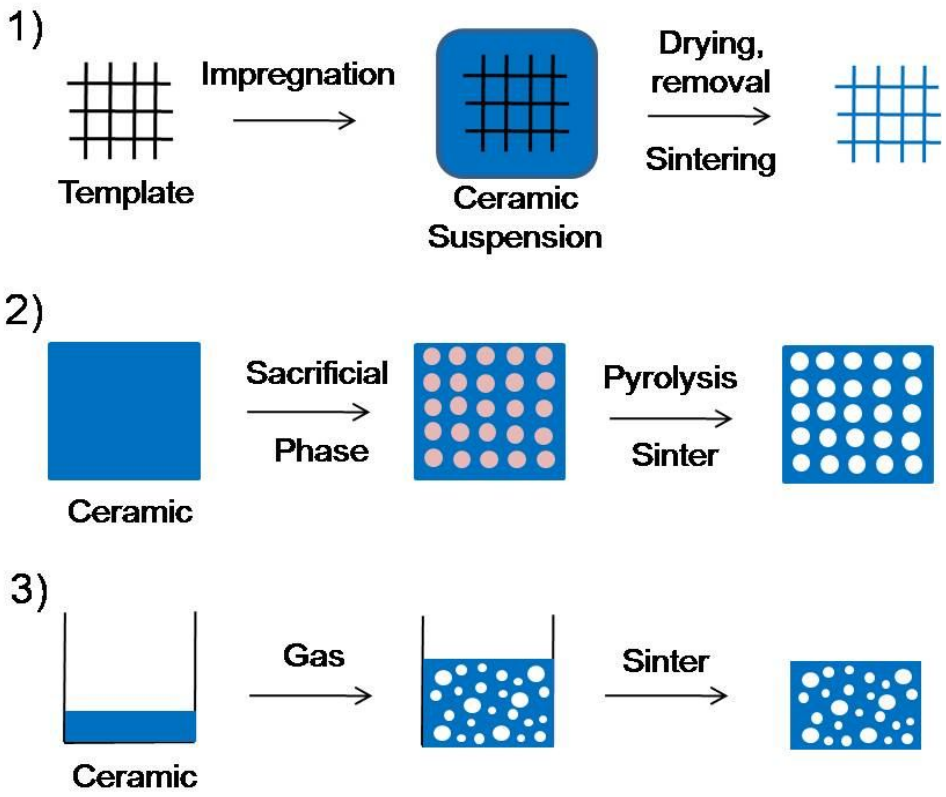

Figure 2-5. Schematics of the three common foaming methods: (1) replica, (2) sacrificial phase and (3) direct foaming.

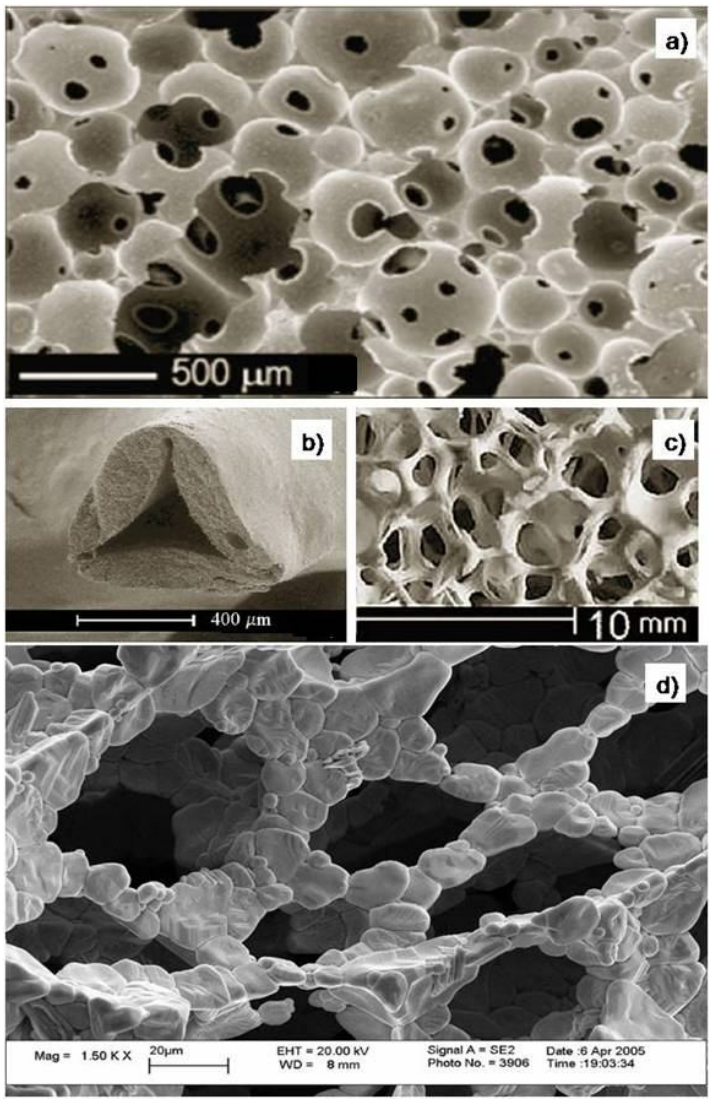

Figure 2-6. Comparison of microstructure in (a) SiOC foam, (b,c) Al_2O_3 foam and d) $BaTiO_3$ foam synthesized via direct foaming method.

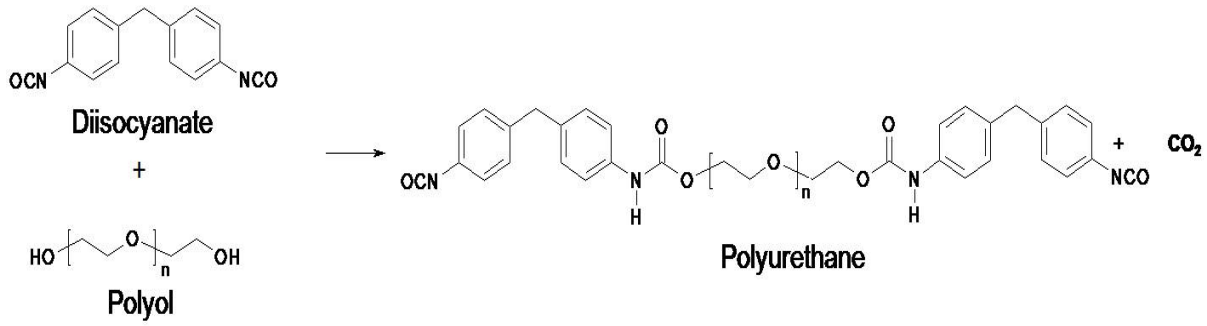

Figure 2-7. Chemical reaction of polyurethane system.

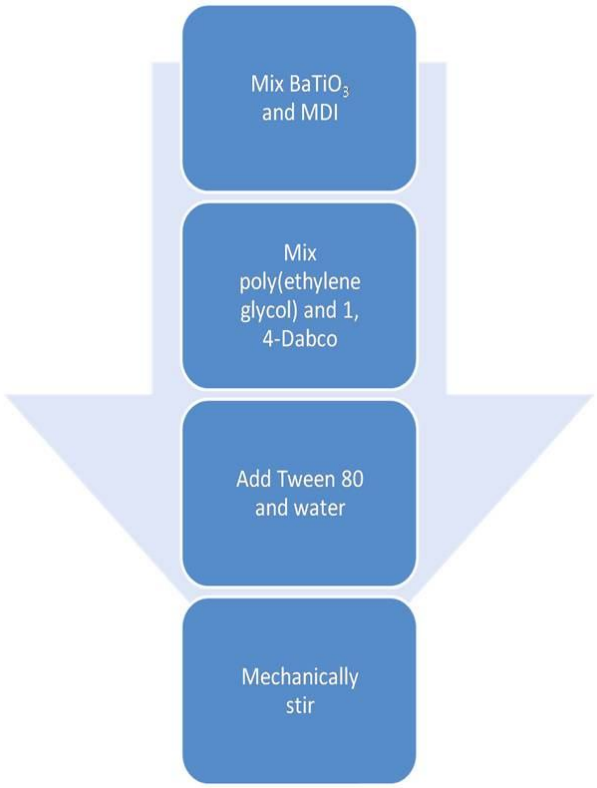

Figure 2-8. Synthesis steps for PU5.

CHAPTER 3
FOAM SYNTHESIS AND MICROSTRUCTURAL ANALYSIS

3.1 Introduction

Foams can be classified by the structure and size of their cell windows. Cell windows in closed cell foams are not interconnected and contribute to their higher compressive strength. Open cell foams contain interconnected cell window networks and are commonly used in composite materials. The Weaire-Phelan structure (Figure 3-1) is theorized to be the ideal unit cell of a perfectly ordered foam, consisting of fitted polyhedra with both hexagonal and pentagonal faces which minimize surface area and maximize packing.[30]

There are three classifications of pore size: micro-, meso- and macroporosity (less than 2 nm, between 2 nm and 50 nm, and greater than 50 nm, respectively).[32] The structure of the foam determines its properties and potential applications. It is characterized in terms of strut characteristics, cell parameters and pore parameters. Cell parameters include grain size and grain boundary integrity of the grain which creates the cell. Pore parameters include cell window size, cell window distribution, and porosity. Strut characteristics are classified by relative density and thickness. It is difficult to classify one “ideal” microstructure for all applications because different applications require different properties and therefore different structures. For example, from a mechanical point of view a smaller grain size and more grain boundaries can lead to increased strength similar to the Hall-Petch effect seen in metals due to dislocation pinning at the grain boundaries.[33] Additionally, lower porosities are preferred to increase compressive strength and the elastic modulus.[34] However, for piezoelectric composites, an increase in porosity would lead to an increase in volume fraction of polymer which would enhance the piezoelectric properties of the composite by transferring stress to the ceramic phase. Grain boundary integrity, dense and sturdy struts without sharp edges and a uniform cell window distribution are desired for both applications.[24,26] By adjusting the synthesis parameters, the microstructure can be controlled to produce various properties for numerous applications.

These synthesis parameters include foaming method, composition, sintering time, and sintering temperature.

The compound $BaTiO_3$ (Chapter 1) has interesting properties including piezoelectric properties. As a foam, $BaTiO_3$ can demonstrate a wider range of properties for additional applications, but has not been investigated in detail like other ceramics. For example, Colombo et al. synthesized flexible and semi-rigid silicon oxycarbide foams from preceramic polymer and a polyurethane system and sintered them at 1200 °C.[25]

A silicon-free commercial polyurethane system and novel laboratory polyurethane system (Chapter 2) have been tailored for barium titanate foam synthesis via direct foaming method. The effects of the synthesis parameters on the resulting microstructures are presented in this chapter.

3.2 Experimental Procedure

The direct foaming method used a liquid, two-component polyurethane system. The fabrication of a polyurethane system (PU) was based on the reaction between a diisocyanate and a polyol (Figure 3-2) which occurs in the presence of a catalyst. To develop a foam structure, water was added as a foaming agent to react with the isocyanate group during the polymerization to produce carbon dioxide, which expands the polymer matrix producing a cellular structure.

To obtain a ceramic-loaded polymeric foam, a ceramic powder was dispersed in the liquid reagents prior to polymerization. $BaTiO_3$ powder (Aldrich, US) with an average grain size of 2 μm and a purity level of 99.99% was weighed to produce specific compositions of 20 vol%, 30 vol%, 40 vol%, 50 vol% or 60 vol%. The same powder was used to test five different polyurethane systems. The five polyurethane systems tested were:

1. PU1 - Rigid commercial system (Prochima, Italy)
2. PU2 - Rigid silicon-free commercial system (Smooth-on, NJ, US)
3. PU3 - Flexible silicon-free commercial system (Smooth-on, NJ, US)
4. PU4 - Rigid diisocyanate concentrated commercial system (Cytec, US)
5. PU5 - Rigid silicon-free laboratory system (University of Rome Tor Vergata, Italy)

The commercial PU systems were combined in ratios of 1:1, polyol to diisocyanate. PU5 samples were prepared using a laboratory developed polyurethane system as described in Chapter 2.[29] Due to chemical importing restrictions, the original polymeric MDI used in the laboratory grade system, Voranate M220, could not be purchased in the United States. Instead, its US equivalent chemical, PAPI 27, had to be used to continue the experiments. Figure 3-3 shows the field emission-scanning electron microscopy (FE-SEM) micrographs of the foams obtained with the two chemicals. No major differences in microstructure were observed. It was concluded that the chemicals were equivalent for this experiment.

The foams were stirred until highly viscous (~ 2 minutes after combining) using an electric screwdriver and stirring attachment and set aside to harden and cure. When dry, the foams were cut into 2 cm^3 rectangular samples.

The newly cut green samples were placed in a 1700 °C horizontal tube furnace (CM Furnaces, Bloomfield, US) designed for air flow to prevent sample reduction and furnace corrosion caused by the burn out of the polyurethane system. The samples were heated at 60 °C/hour to 600 °C to prevent damage to the struts and held for 1 hour to completely remove the polyurethane from the foam. Once the polyurethane is removed, the system is completely ceramic. It was then heated at 160 °C/hour to a specific sintering temperature and held for either 4, 8 or 15 hours. The temperature was lowered at 140 °C/hour to room temperature. All samples were fired in air with the flow rate maintained at 10 cm^3/minute. A flow chart is shown in Figure 3-4 to organize all of the potential variables. Depending on the type of structure that is

produced from each of these variables, some were eliminated, which simplified the experiments. This will be discussed in the next section.

FE-SEM was used to determine the effect of synthesis parameters on relative grain and cell window sizes and relative grain and cell window size distributions. Four images of different magnification (100X, 500X, 1000X, and 5000X) were taken of each sample at different locations of the sample. Three samples of each PU system were characterized to determine how repeatable the process was. This was a very important part of the project to determine the interrelationship between processing, structure and properties of the foams. If the structure was not repeatable, these relationships would be insignificant.

Optical analysis was performed using Image J software on the resulting SEM images. Parameters determined from this technique were average cell window area and average grain area. Three images for each variable configuration (i.e. PU2, 30 vol%, 1400 ^{o}C for 8 hours) at 1000X magnification were used in the analysis. In addition images were taken and two different depths into the sample to ensure a homogeneous structure. Each of these depths was analyzed as well.

The grain boundaries and cell windows were outlined in black using an image editing software, while the grains remained light gray. The threshold of the image was then adjusted to highlight the dark regions or lights regions based on extreme contrast. For example, if the grains were being analyzed, the threshold settings would make the grains red and the grain boundaries and cell windows white. The macro, “Analyze Particles”, was used to scan the image, line by line, counting red as “1” and white as “0” and starting a recount every time a white pixel was encountered. The program then sums the count and presents it in a table with statistics including average and standard deviation. The resulting number of pixels per red region was then converted to microns per grain using the image magnification to determine an average grain area or cell window area. From these values an average cell window and grain size were estimated assuming that the grains and the cell windows were circular (size =

$(\pi/2)^{1/2}$). Using this technique an estimate of the grain and cell window sizes was determined. Cell size was not calculated since the resulting microstructures did not produce cells. More description on this analysis is given in Appendix A.

The values of the cell window sizes were more accurately measured using a helium pycnometer (Quantachrome Ultrapyc 1000 Gas Pycnometer) and mercury porosimetry (MP). Helium pycnometry measures the true density and calculates the open porosity which is important to create the 3-3 piezoelectric composite. MP characterizes the pore size distribution taking into account both the pores in the grains and struts and the cell windows. Raman spectroscopy was performed to determine if residual stress was present in the foam structure, compared to bulk barium titanate. The results are shown in Appendix B.

All of the results from the characterization techniques were compiled to determine the ultimate processing parameters that would produce and open structure with dense struts and no sharp wall edges.

3.3 Results and Discussion

Figure 3-5 shows the difference in microstructure between PU1 and PU5 foams. The presence of Si-rich contaminants (Figure 3-5A) created platelets at the grain boundaries. These contaminants could be detrimental for mechanical properties because it decreases the mechanical strength of the grain boundaries and electrical applications by decreasing the charge mobility at the grain boundary. Therefore, the Si-free PU5 system was successfully developed to avoid contaminants (Figure 3-5B) and Si-free commercial systems were purchased. In order to understand the process-structure relationship, each synthesis parameter was examined to determine its influence on the foam microstructure.

3.3.1 Effect of Sintering Time and Temperature

The microstructure is influenced significantly more by sintering temperature than by sintering time (4, 8 and 12 hours). Experiments varying in sintering temperature were optimized for PU5 laboratory grade (using Voranate M220), 20 vol% samples sintered at 4 hours. The sintering

temperatures tested were 1250, 1300, 1350 and 1400 °C. High and low magnification SEM images of this system are in Figure 3-6 and Figure 3-7, respectively.

A well-defined, open cell microstructure is maintained at lower sintering temperatures (1250 and 1300 °C) while at higher sintering temperatures the cell windows sometimes lack spherical geometry, which is also controlled by sintering time and composition. The cell window size and porosity decreased with increasing temperature. High temperature samples are more robust during handling than low temperature samples. This is because the low temperature samples do not have well sintered structures which weaken the mechanical resistance. Because of its more uniform cell window and grain size distributions, handling capabilities and well-sintered structure, a sintering temperature of 1400 °C was used for all other experiments involving different synthesis parameter variations.

The foams synthesized via direct foaming method with PU2 and PU5 follow conventional mechanisms regarding sintering and foam formation. The stages of sintering (initial, intermediate and final) can also be seen in Figure 3-7. At lower temperature (initial), there are no neck formations, but the contact area between particles increases. As the temperature increases (intermediate), continuous cell window and cell channels form and necks increase. Finally at 1400 ^{o}C, smaller cell windows between the grains are eliminated and grains are consolidated. Note the well distributed grain sizes in the 1400 ^{o}C samples in Figure 3-6D and Figure 3-7D, respectively.

The microstructure exhibits normal grain growth, as the grain size is proportional to the square root of the sintering time. As expected, there is a difference in grain size between samples sintered for 4 hours and samples sintered for 8 hours. At 4 hours, the grain size is 25 to 75 % smaller than at 8 hours. There is less unsintered material at higher sintering times. However, there is little difference in microstructure between 8 hours and 15 hours except in a slightly increased grain size, 5 to 10 %. A sintering time of 8 hours for all foams was primarily

chosen because it produced a homogeneous microstructure in less than 2 days of total processing time. The differences in microstructure are shown in Figure 3-8 for PU5 foams.

3.3.2 Effect of Polyurethane System

Of all the processing parameters, the choice of polyurethane system had the most significant impact on the resulting microstructure of the foam. It determined the configurations and connectivity of the foam while the other parameters such as composition and sintering temperature affect the size and shape of the grains, struts and cell windows. Because each PU was compositionally different, so were the foams.

PU1 (Figure 3-9A and B), PU3 (Figure 3-9E and F) and PU4 (Figure 3-9G and H) foams all had cells with some closed porosity (> 5%). PU2 (Figure 3-9C and D) and PU5 (Figure 3-9I and J) foams created very open structures (closed porosity < 5%) which prevented them from creating cells; therefore the structures only consisted of struts and windows. PU1, PU2 and PU5 all exhibited a unique structure characteristic which differs from the microstructure of foams previously reported in that they have struts which consist of a few larger grains (> 15 μm) rather than many smaller grains (< 5 μm).

After preliminary research, some of the PU systems were eliminated because they did not provide homogeneous foam structures in terms of uniform cell, grain and cell window sizes and uncontaminated grain boundaries. PU1 foams contained rod contaminants at the grain boundaries, thin struts, and did not produce uniform grain size of cell window size distributions. PU3 foams, while very strong comparatively to the other foams, produced low porosity and closed cell structures which were not conducive to 3-3 composites. PU4 foams demonstrated abnormal grain growth with a contrast between very large grains (>20 μm) surrounded by hundreds of very small grains (<2 μm) and sharp cell wall edges which contributed to their sensitivity during handling. This is due to the increased stress concentrations created at sharp and small areas such as the wall edges. Thick, dense and rounded struts prevent these stress concentrations, making the foams easier to handle. The final PU systems investigated were

PU2 and PU5 foams. The remaining characterization techniques including image analysis, helium pycnometry and MP were used to only characterize these final PU systems.

Although both maintain shape during handling and produce homogeneous microstructures, PU2 and PU5 foams have considerably different microstructures. PU2 foams have smaller grain sizes (20 – 27 μm), larger and more interconnected cell windows (87 – 98 μm) and struts consisting of many smaller grains (Figure 3-9C and D), all of which increase its resistance to damage during handling and mechanical strength.

PU5 foams have larger grain sizes (35 – 52 μm), smaller cell windows (39 – 76 μm) and struts consisting of a few large grains (Figure 3-9I and J). Due to the smaller cell window size and larger grain size, PU5 foams are 3% denser and therefore can be handled easily as well. Image analysis data and MP data reflect these trends in grain, cell window and pore size, shown in Table 3-1 and Table 3-2. The minimum values reported for the MP data in Table 3-3 reflect the pore sizes in the strut and the maximum values reflect the cell window sizes.

Additionally, PU2 exhibits well-defined grain boundaries and hexagonal grain terraces, indicating growth in the <111> direction. PU5 samples have smoother and more abnormally shaped grains. The terraces on the faces of the grains could possibly indicate over-sintering and could potentially decrease mechanical strength. The well-defined grain boundaries are preferred for higher mechanical strength because they indicate a that the foams have reached the final stage of sintering since the atoms have had more time to diffuse away from grain boundaries, producing deeper and well-defined grain boundaries. However, the smooth, abnormally shaped grains could potentially decrease the stability for the foam. It is proposed that the difference in microstructure between the foams is derived from the difference in chemical composition of the PU systems. The type of diisocyanate, polyol and the inclusion of pore minimizers or catalysts can all affect the microstructure. There are many different types of diisocyanates and polyols which can be used to create polyurethane. For example, methyl diphenyl diisocyanate (MDI), used in PU5, is a symmetric diisocyanate which produces very rigid foams. It reacts very quickly

which limits the number and size of bubbles introduced into the foam. Pore minimizers, such as Tween 80, and catalysts also have the same effect. The inclusion of an MDI and Tween 80 make PU5 foams denser that PU2. Unfortunately, the exact chemical composition of most commercially available PU systems and their components are not publicly available.

In the work by Colombo et al.[13], SiOC foams were created using preceramic polymers and a PU similar to PU5. Flexible, semi-rigid and rigid foams were synthesized and characterized. These foams had cellular structures similar to the flexible foams made with PU3, but exhibited increased porosity and homogeneity. In comparison to PU2 and PU5 foams, the SiOC foams have interconnected cell structure and more closed cells while the foams focused on in this paper have an interconnected cell window structure and open cells. While the struts are denser in the SiOC foams due to the formation of cell walls, they also have very sharp edges, which could lead to a decrease in mechanical strength. Both the SiOC and $BaTiO_3$ foams demonstrate macroporosity.

3.3.3 Effect of Composition

In both types of foams, the most homogeneous microstructures in terms of cells, grains and cell windows were found at 30 vol% of barium titanate. Below or above this value, the integrity, defined as microstructure homogeneity of the foams, decreased. Increasing ceramic concentration resulted in increased abnormal grain growth, increased amount of unsintered material, and very large grains (> 2000 μm^2). These samples usually result in an average grain area that does not reflect the actual microstructure since it includes a large range of grain sizes, from less than 3 μm for unsintered particles to greater than 400 μm for large grains. It is suggested that the difference in grain size caused by the difference in composition is due to how the powder is dispersed into the PU. At lower compositions, the powder can be dispersed homogeneously with more room to grow at the same rate during sintering. However, if the composition is too low, the material does not sinter as thoroughly because contact between particles is limited and at higher compositions, oversaturated PU doesn't allow the particles to

sinter and grow at constant rates. Porosity is influenced by ceramic content. An increase in ceramic content results in a decrease in porosity as seen in Table 3-3 and Table 3-4.

There is a more significant decrease in cell window size and increase in grain size with increasing $BaTiO_3$ content in PU2 than in PU5 shown in both the SEM images in Figure 3-10 and Figure 3-11 and the image analysis data in Table 3-1 and Table 3-2.

Additionally, uniform cell window size distributions and open structures are more commonly produced at 30 vol% than any other composition. Moreover, the PU mixture becomes inhomogeneous and oversaturated at higher $BaTiO_3$ concentrations (Figure 3-11C and D) which cause unsintered particles to contaminate the grain boundaries. However, increased ceramic concentration produces stronger and less brittle foams. At 20 vol%, PU5 foams are very brittle and break during handling. Comparatively, at 50 vol%, PU2 foams are very durable and can withstand extensive handling. A ceramic content of 30 vol% give a good compromise between these two properties. Physically, PU2 and PU5 foams behave similarly when handled.

3.4 Conclusion

A surfactant-stabilized direct foaming method was used to create $BaTiO_3$-based ceramic foams. The composition, polyurethane system, sintering temperature and sintering time were varied to determine their influence on the microstructure of the foam and ultimately the properties and applications of the foam. After determining that Si-based PU systems produced contaminants at the grain boundary and inhomogeneous grain size distributions and flexible PU systems produced closed cell structures, research was focused on Si-free, rigid PU systems: one commercially available and the other laboratory developed. After additional initial testing, some of the other variables were eliminated. The primary synthesis variables were polyurethane system (PU2 – commercial and PU5 – laboratory) and composition (20 – 60 vol% ceramic).

Both the rigid commercial and rigid laboratory systems produced foams with uniform cell window size distributions and dense, thick struts. However, the commercial system's struts consisted of many small grains which should have better mechanical properties, while the

laboratory system struts had fewer but larger grains. The rigid laboratory developed system demonstrated uniform cell window distribution, variable porosity (75 - 87 %), dense struts, contaminant-free grain boundaries at concentrations less that 50 vol% and mechanical integrity. The commercial silicon-free system also had a uniform cell window size distribution, smaller grain size, larger cell window size and also demonstrated dense struts and variable porosity (82 – 93 %).

Lower ceramic concentrations (20, 30 and 40 vol%) are ideal for electrical applications because of the interconnected cell window network and increased porosity. However, they are more brittle than foams with higher ceramic concentrations (50 and 60 vol%) which are more favored in mechanical applications. Foams with 30 vol% ceramic demonstrated a homogeneous microstructure with a balance of properties for both mechanical and electrical applications. They have high porosity (~ 88 %), uniform and smaller grain size, are relatively strong and not easily damaged.

A 30 vol% foam, synthesized using the laboratory developed rigid polyurethane system and a 30 vol% commercial silicon-free system, sintered for 8 hours at 1400 °C, produced different microstructures which have the potential to be used in electromechanical applications.

Table 3-1. Image analysis grain data.

PU	Composition (vol%)	Average Grain Area (μm^2)	Standard Deviation (μm^2)	Average Grain Size (μm)
PU2	30	1244	100	20
PU2	40	1563	121	22
PU2	50	1662	366	23
PU2	60	2290	298	27
PU5	20	3849	384	35
PU5	30	7178	285	44
PU5	40	6165	327	48
PU5	50	8495	327	52

Table 3-2. Image analysis cell window data.

PU	Composition (vol%)	Average Grain Area (μm^2)	Standard Deviation (μm^2)	Average Grain Size (μm)
PU2	30	1244	100	20
PU2	40	1563	121	22
PU2	50	1662	366	23
PU2	60	2290	298	27
PU5	20	3849	384	35
PU5	30	7178	285	44
PU5	40	6165	327	48
PU5	50	8495	327	52

Table 3-3. Mercury porosimetry data.

Sample	Minimum (μm)	Maximum (μm)	Porosity (%)
PU2-30-8	4.9	111	92
PU2-40-8	4.7	97	86
PU5-20-8	4.6	80	93
PU5-30-8	4.3	69	88

Table 3-4. Porosity measurements by helium pycnometer.

Polyurethane System	Composition (vol%)	Porosity (%)
PU2	30	93
PU2	40	90
PU2	50	88
PU2	60	82
PU5	20	87
PU5	30	85
PU5	40	83
PU5	50	75

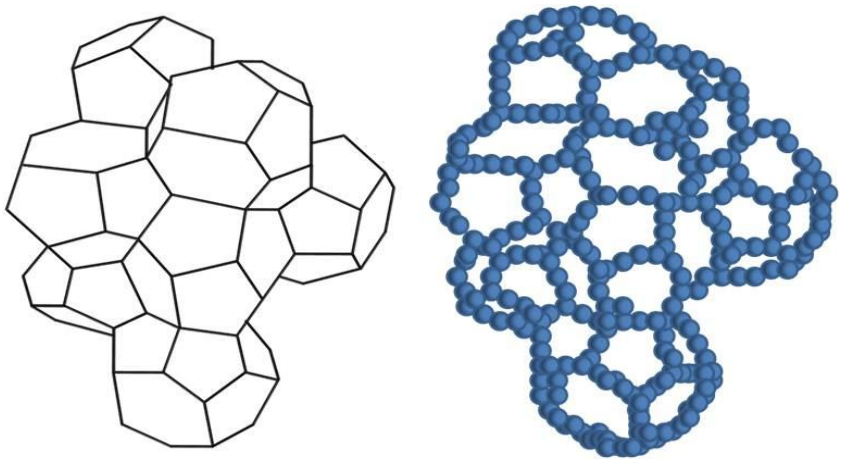

Figure 3-1. Weaire-Phelan schematic.

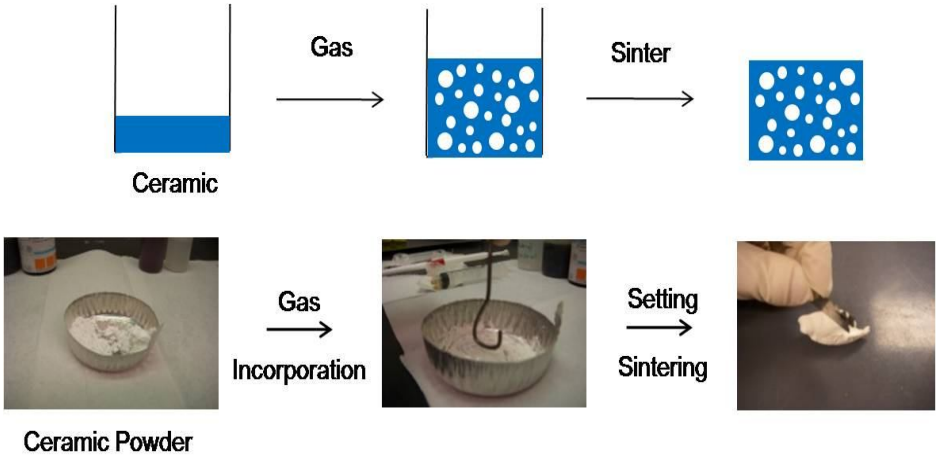

Figure 3-2. Direct foaming schematic using barium titanate powder.

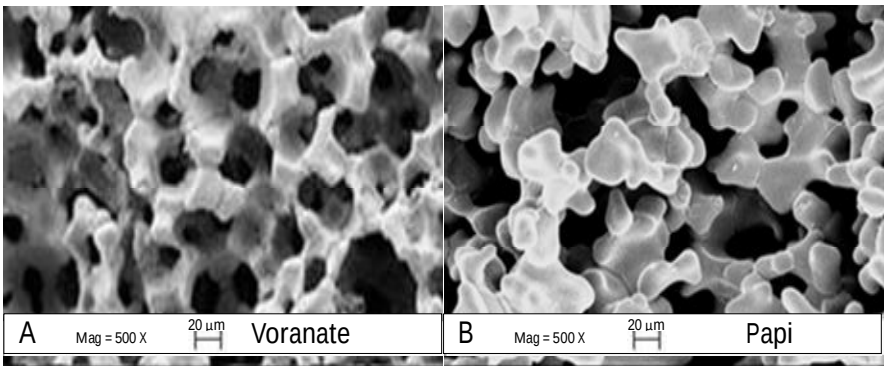

Figure 3-3. FE-SEM images of PU5 sample synthesize with (A) Voranate M220 and (B) PAPI 27 both sintered at 1400^{o}C for 4 hours.

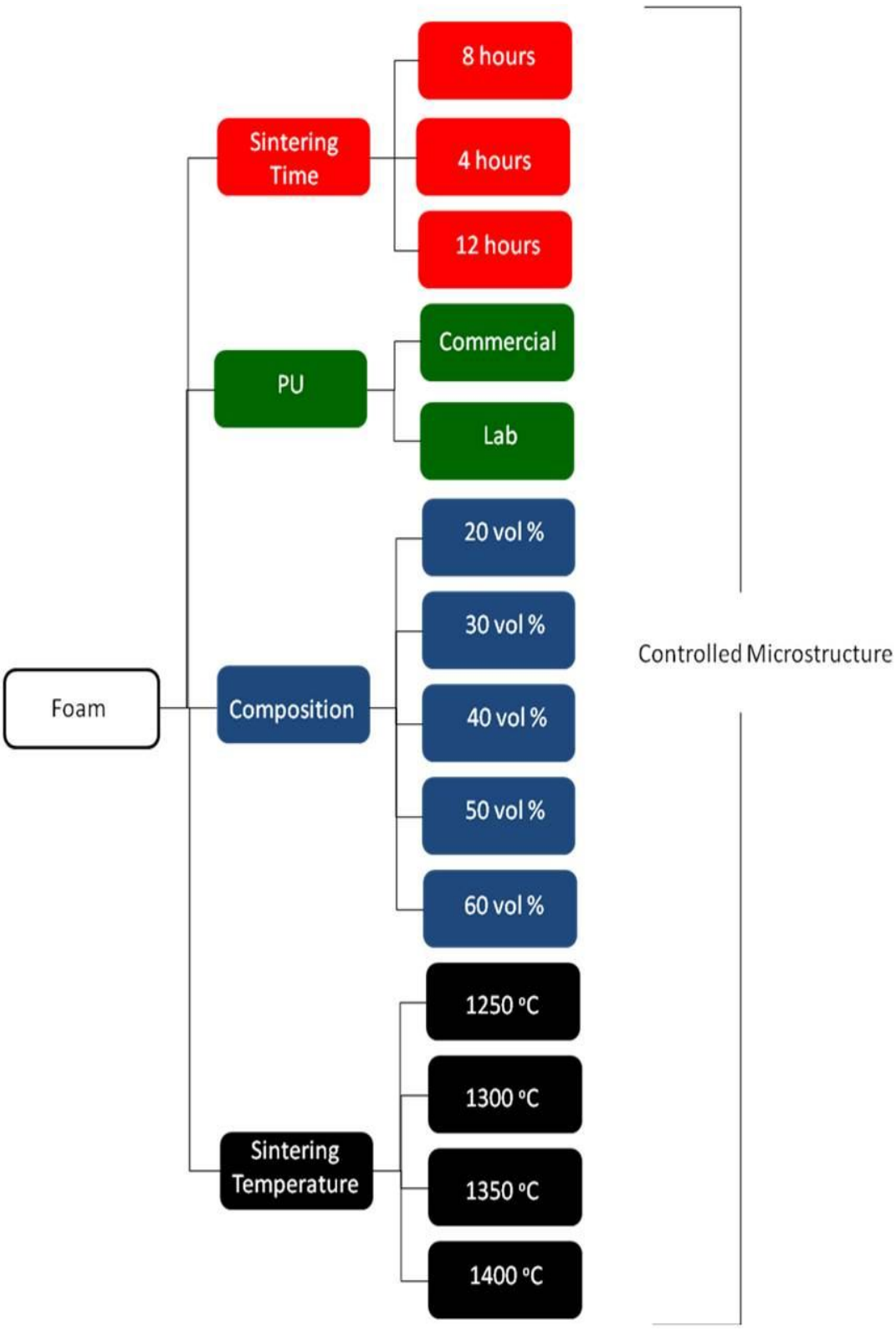

Figure 3-4 Processing parameters chart.

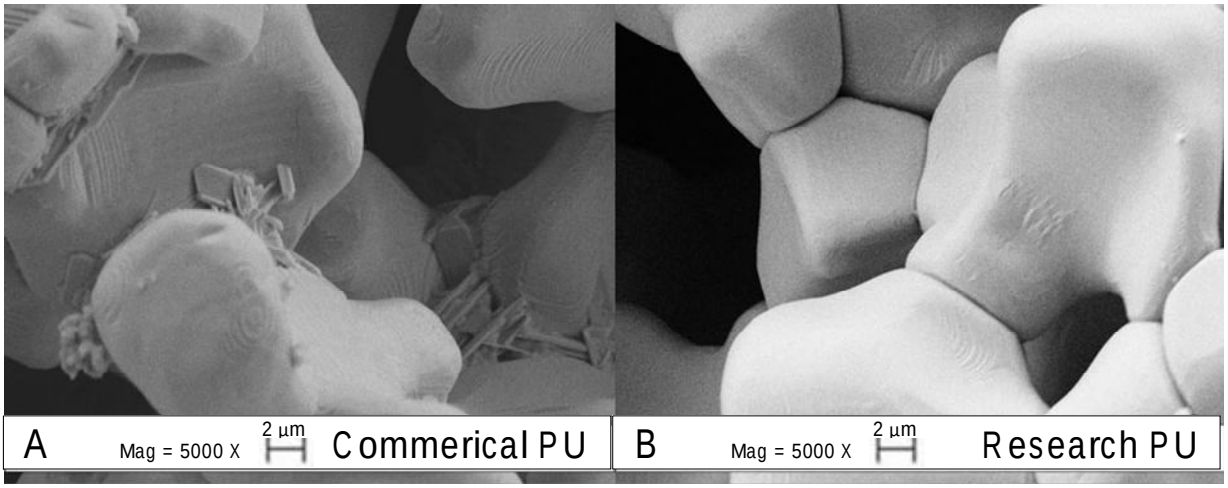

Figure 3-5. FE-SEM images of (A) $BaTiO_3$ foam synthesized using PU1 and (B) foam synthesized using PU5.

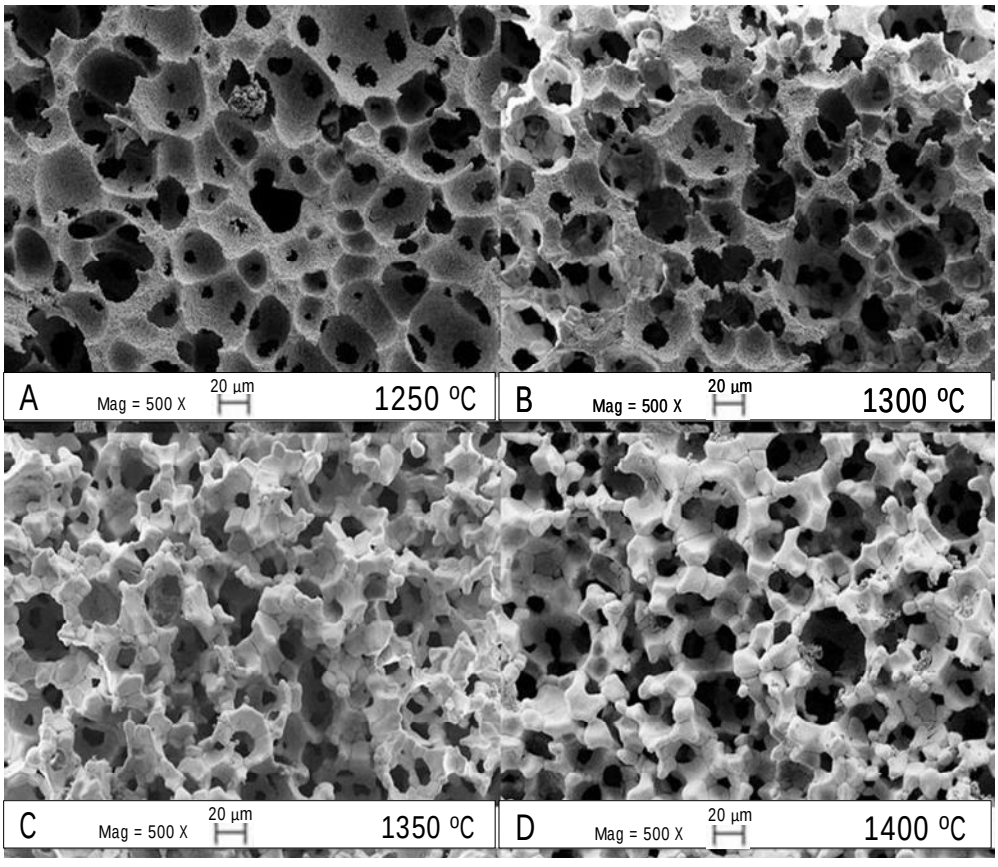

Figure 3-6. FE-SEM micrographs of PU5 20 vol% samples sintered at different temperatures for 4 hours in low magnification.

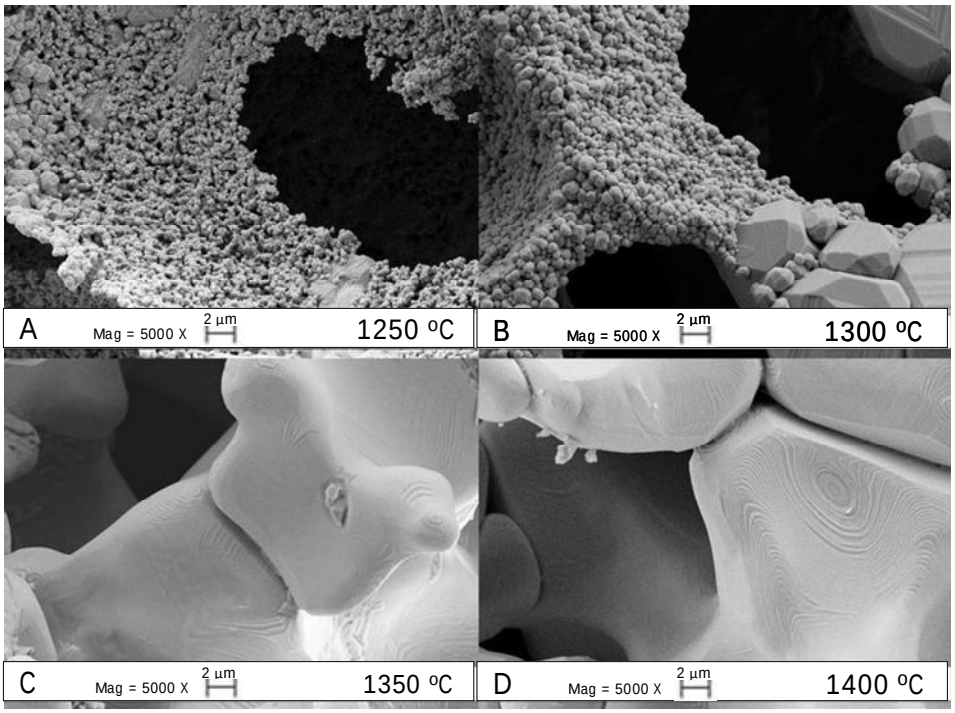

Figure 3-7. FE-SEM micrographs of PU5 20 vol% samples sintered at different temperatures for 4 hours in high magnification.

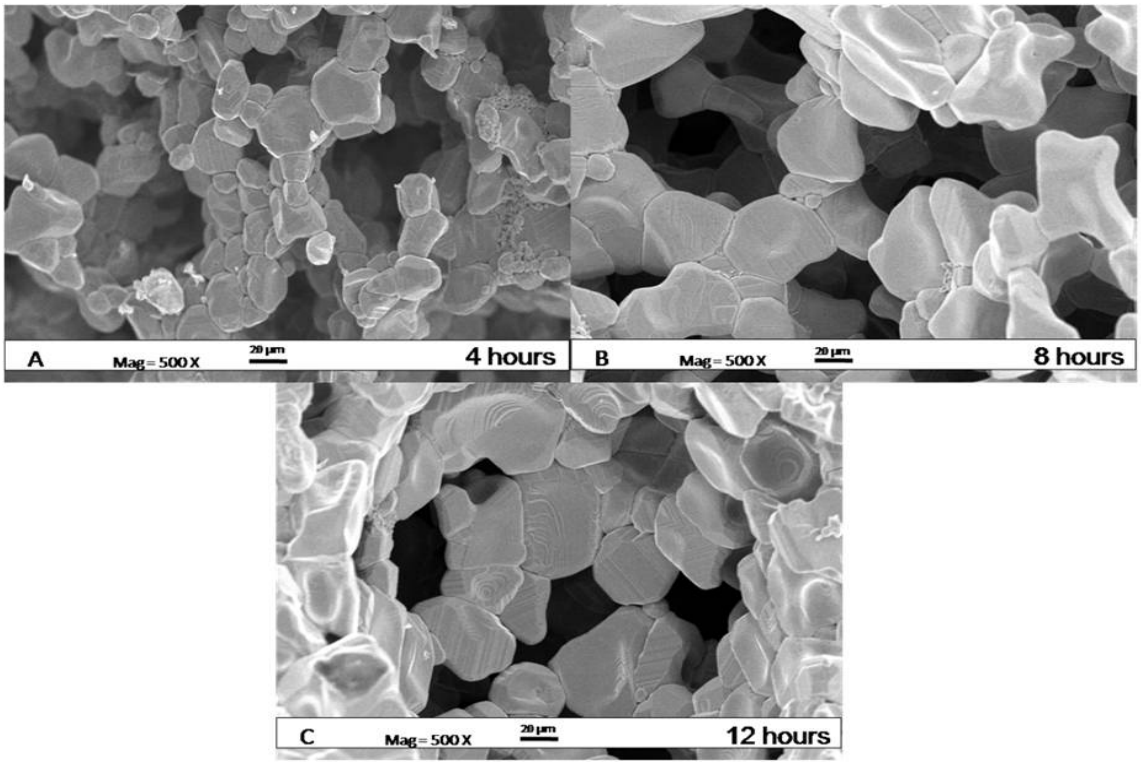

Figure 3-8. FE-SEM micrographs of PU5 30 vol% samples sintered at different times A) 4 hours, B) 8 hours and C) 12 hours**.**

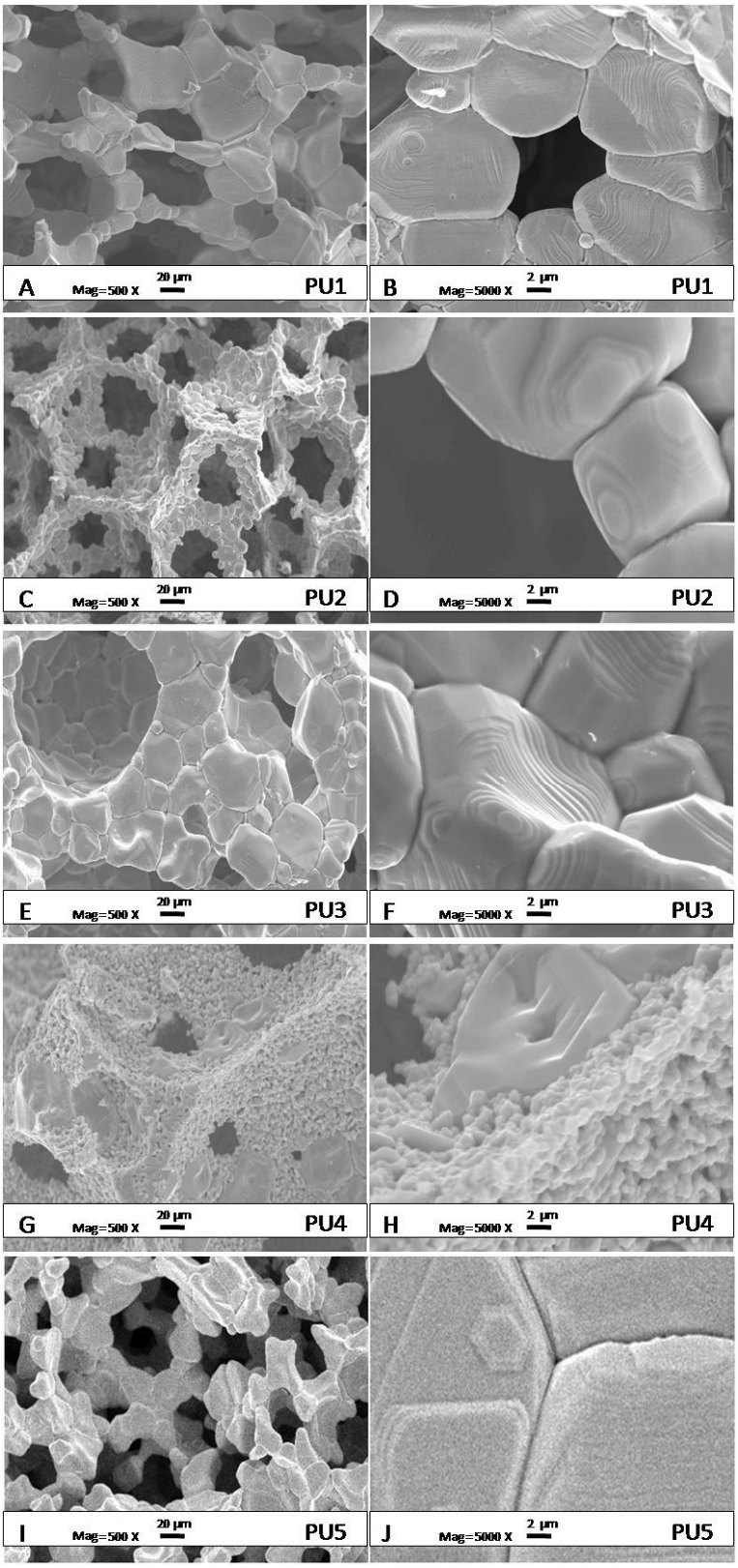

Figure 3-9. FE-SEM images at 500X and 5000X of (A,B) PU1 (C,D) PU2 (E,F) PU3 (G,H) PU4 and (I,J) PU5 foams.

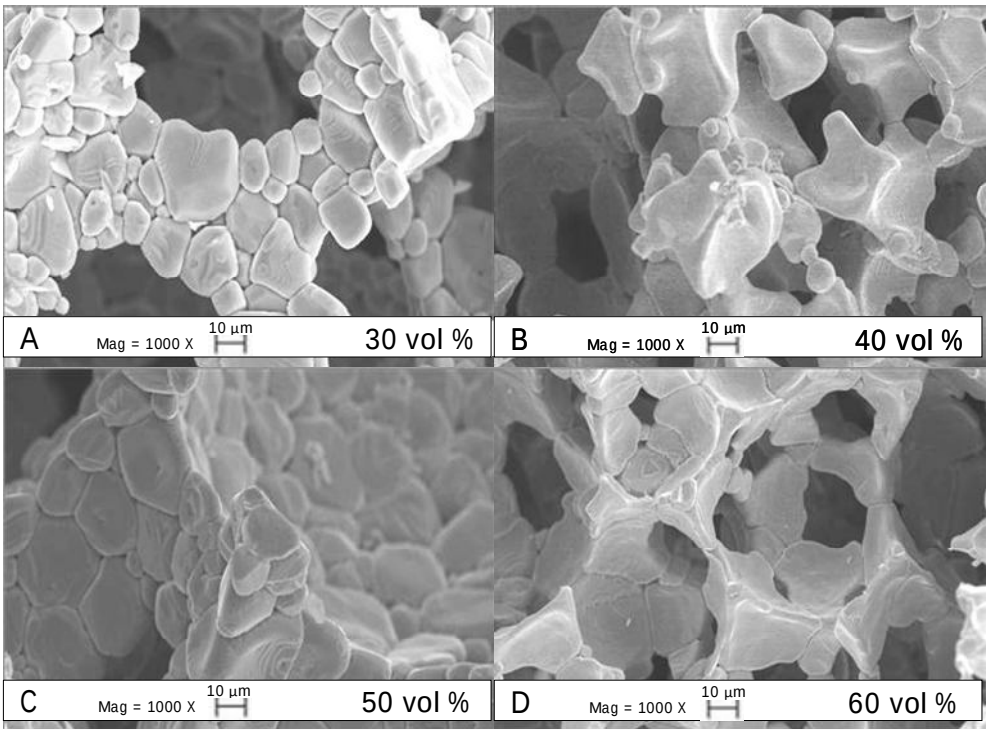

Figure 3-10. FE-SEM images of PU2 foam samples at (A) 30, (B) 40, (C) 50 and (D) 60 vol% sintered at 1400 °C for 8 hours.

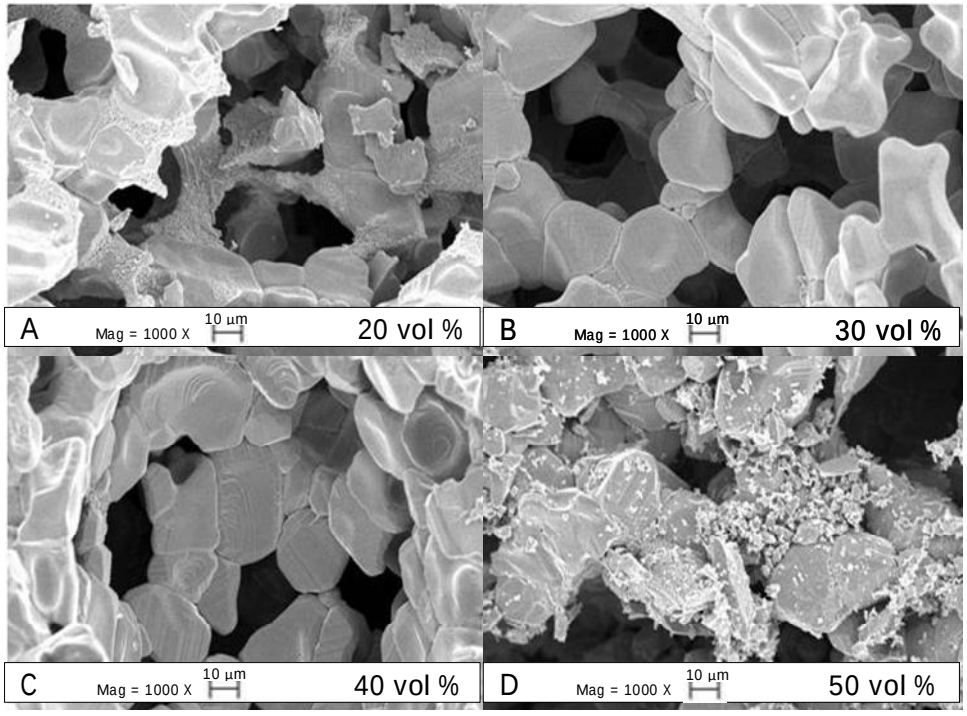

Figure 3-11. SEM images of PU5 foam samples at (A) 20, (B) 30, (C) 40 and (D) 50 vol% sintered at 1400 °C for 8 hours.

CHAPTER 4
MECHANICAL CHARACTERIZATION

4.1 Introduction

As discussed in Chapter 3, $BaTiO_3$ foams were synthesized using the direct foaming method based on two different rigid, Si-free polyurethane systems, a commercially purchased system (PU2 = CPU) and a laboratory developed system (PU5 = LPU). It was found that the microstructure of the ceramic foam could be controlled by adjusting the polyurethane system, ceramic composition, sintering time and sintering temperature. An open-structure foam with dense, rounded struts composed of a few larger grains (20 – 45 μm) was produced at a high sintering temperature (in comparison to bulk) and an intermediate sintering time.[34] The optimal ceramic content was determined to be 30 vol% and the PU made up the remaining 70 vol%. It was found that the variability in density for these foams was not significant.

Although these foams are primarily intended for sensing application, their ability to withstand stress and deformation is important for handling purposes as well as to ensure mechanical integrity at high stress levels during service. Among many desirable properties, the compressive behavior is of prime importance. In literature, mechanical properties of 1-3[35] and 0-3[22] composites have been reported but very little has been reported on mechanical properties of 3-3 composites. A typical 1-3 composite consists of rods in a matrix in which ceramic rods are held parallel by a passive polymer matrix.[35] For underwater sensor application it is important that the acoustic impedance of the composite be similar to that of water (1.569 MRayls).[4] While recent breakthroughs have been made with 1-3 composites in achieving this low acoustic impedance[5], 3-3 composites offer a good balance between a polymer with low acoustic impedance and a piezoelectric ceramic with high mechanical strength and piezoelectric properties. However, for good mechanical stability, the strengths of both the ceramic foam and the polymer must be enhanced.

In this study, the mechanical properties of the ceramic foam synthesized via the process previously discussed in Chapter 3 were measured. For the piezo-sensor application, the primary focus is on the elastic response because reversible deformation is required for the sensor to operate. In this work it is shown that the mechanical properties of the foam fabricated by the above mentioned method are comparable to other ceramic foams and therefore, possibly suitable for sensor applications.

For polymeric foams, Liu and Subhash[36] proposed a phenomenological model that can capture the entire compressive stress-strain response. In general, the stress-strain response of porous materials subjected to compressive loads has three distinct zones; (i) an elastic region, (ii) a plateau region and (iii) a densification region. The plateau region is associated with the collapse of the porous, cellular structure which gives the foam its energy absorption ability. As mentioned previously, for the piezo-sensor application, the primary focus is on the elastic region due to the requirement of reversible deformation. Therefore, only the early portion of the stress-strain response that includes elastic and partial collapse strains were used for modelling and property determination.

4.2 Experimental Procedure

$BaTiO_3$ foam samples were synthesized using two rigid, Si-free polyurethane systems: (i) commercially purchased (CPU, previously PU2) from Smooth-On (Easton, PA) and (ii) laboratory developed system (LPU, previously PU5) by Traversa et al.[29], at the University of Rome – Tor Vergata. After the previously reported processing steps, 28-32 vol% $BaTiO_3$ was foamed and sintered for mechanical testing.[34]

$BaTiO_3$ foams produced from the above two systems were cut into 12.7 mm diameter specimens using a tape cast hole punch. Five specimens were made for each system. The density of the foam was systematically varied by varying the ceramic content from 28 – 32 vol%. It was earlier found that the variability in density from one specimen to another was small (0.08%) when the initial ceramic content was kept constant; therefore, only one sample was

made for each density and the difference in mechanical properties of foams produced from the two PU systems was determined. The apparent density and open cell porosity of each specimen was measured using helium pycnometry (Table 4-1). It is shown that the LPU foams were denser due to a smaller expansion during the foaming process but they also have a larger change in density with corresponding change in ceramic content, compared to CPU foams. Uniaxial compression experiments were performed at room temperature using a MTS universal testing machine (UTM). Each specimen was marked with a grid of horizontal lines to track the uniformity of deformation during the test. Previously, it was noted that when these foam specimens were loaded without any lateral confinement, they deformed unevenly along the length of the specimen.[37] This behavior was due to premature collapse of large porous cells that lie along the outer surface. The collapse the led to instabilities resulting in buckling of the entire specimen. Such buckling modes are also observed in commercial brittle polymer foams. To avoid this mode of failure it was decided to test the specimens in a transparent confinement cell as shown in Figure 4-1.

The transparent cell was made of acrylic and consisted of a central cylinder with an end cap that can be screwed to the bottom of the cylinder. The ceramic foam specimen is placed inside the cell and pushed to the bottom by a cylindrical rod. The entire assembly is placed in the MTS machine and loaded at a displacement rate of 1.27 mm/min resulting in a strain rate of 0.001/s. It is assumed that the strain of the acrylic rod is negligible.

The experimental data was then fit using the phenomenological model proposed by Subhash and Liu[36] further discussed in Section 4.3.3.

4.3 Results and Discussion

4.3.1 Confined Compression Testing

Because the foams were fabricated using the process described in Chapter 3 the microstructure is similar. The ceramic content was varied around an average of 30 vol% to determine the effect of density on the mechanical properties of the foams. Both PU foams are

resilient during handling and produce homogenous microstructures as determined from SEM and image analysis previously reported by the author and collaborators[34]. CPU foams had larger and more interconnected cell windows (98 μm) and struts consisting of a few intermediate grains (20 μm), while LPU foams had smaller cell windows (67 μm) and struts consisting of a few large grains (45 μm).[34]

The compressive engineering stress-strain responses of the different ceramic foams are shown in Figure 4-2 and Figure 4-3. Because the focus of the work was on the elastic region of the response, the samples were strained below 60% (to the yield point). Similar to any cellular material behavior, the ceramic foams exhibited an initial elastic response followed by a cell collapse process which results in the plateau region. If the foams were compressed further, a densification response probably would have been observed. The stress-strain response was strongly dependent on initial foam density. Both the initial slope and the collapse stress increased with density for both PU systems. The slopes were highly non-linear and therefore the stiffness was incrementally calculated and averaged over the elastic range. This stiffness is known as the collapse stress (σ_C).

Mechanical properties extracted from the above plots are summarized in Table 4-2. The compression modulus (E_C) and collapse stress (σ_C) of the CPU and LPU foams determined from the above stress-strain responses are plotted with respect to density in Figure 4-4. Although both material properties increase with increasing density for both foams, a significantly higher rate of increase is observed in foam produced by LPU. As expected, the LPU foam had on average a higher modulus and collapse stress due to higher density. The mechanical properties for both of the ceramic foams follow a linear trend with density. A better comparison of mechanical properties of foams can be seen in Figure 4-5 where the stress-strain curves at two different foam densities are compared. Clearly, for approximately similar foam density, a greater collapse stress is observed in LPU foam than in CPU foam in addition to a greater increase in properties with a similar increase in density. In addition, at both densities, it can be

seen that the mechanical properties of the foams made with LPU are higher than the foams made with CPU.

As mentioned earlier, the foams were marked with grid lines to track the uniformity of deformation and collapse the collapse process. Figure 4-6 and Figure 4-7 illustrate the deformation behavior of foams at various strain levels. Note that all these lines remain relatively straight throughout the deformation process. In foams with relatively large cell window sizes and inhomogeneous microstructures, these lines become nonlinear and the spacing between the lines becomes uneven very early on in the deformation process due to the collapse of isolated large cells.[36] Such features were not observed in the $BaTiO_3$ foams because the cell window size is relatively small and uniform and therefore, the spacing between any two lines remains relatively constant along the length. However, the spacing between the lines decreases with strain as the cells start to collapse uniformly.

There is one noticeable difference between the deformation behavior of LPU and CPU foams. In the LPU foams, the deformation is not uniform along the length of the specimen. Note that the line spacing on the top decreases more rapidly than the spacing at the bottom. This indicated that the deformation in this foam is more progressive rather than uniform throughout the specimen. The deformation progresses from the top of the specimen to the bottom of the specimen with increasing load, i.e., there is a progressive collapse of cells with load. On the other hand, the deformation of CPU foams is comparatively more uniform (Figure 4-7) as indicated by the continued reduction in the spacing of most of the lines with increasing strain.

Table 4-3 compares the properties of the selected $BaTiO_3$ foam to two other ceramic foams of similar densities and a bulk material commonly used in commercial sensors[41]. The open cell, macrocellular SiOC foam was synthesized by Colombo et al. via direct foaming method using a PU similar to LPU.[38] The collapse strength of the SiOC foams is higher while the densities are similar because the structures are different. The SiOC foams have more closed cell porosity and a much smaller cell window size (< 20 μm), while the $BaTiO_3$ foams have significantly more

open porosity and a larger window size (40 – 80 μm). These features make the $BaTiO_3$ foam a better candidate for a piezocomposite. The LPU foam at the same density has a higher collapse stress due to denser struts, while the cordierite foams have hollow struts caused by the replica process.[39]

The $BaTiO_3$ foam struts have an average thickness of 60 μm and consist of a few intermediate sized grains (~ 20 μm), determine using image analysis of SEM images as described in the previous chapter. In comparison, the SiOC have struts consisting of many small grains which are greater than 60 μm thick. According to Li et al.[40], the thickness of the cell wall or strut is directly correlated with the strength of the foam; therefore, all other being equal, it is expected for the strength of the other foams to be higher due to thicker struts than the $BaTiO_3$ foam. Most piezo-sensors in the market today are made of bulk electroceramic materials such as PZT and have higher mechanical strength. The foams presented here will be infiltrated with a polymer to enhance mechanical properties and possibly piezoelectric properties depending on the polymer selected.

The required mechanical strength of a piezoelectric material for sensor applications is yet to be reported. While the mechanical properties of the $BaTiO_3$ foam skeleton are not yet comparable to other composites, such as the 1-3 ceramic rod composites by Smith et al.[5] (E~31 GPa for 25 % PZT rod composite), the ceramic foam could still be acceptable for sensor applications and will be determined once a prototype piezocomposite sensor has been fabricated. It must be noted that the mechanical properties of the foams presented here are not yet optimized. The primary focus is to produce 3-3 piezocomposites with enhanced piezoelectric properties before optimizing the mechanical properties and ensure that the material can withstand the stress required for this application. While the stress required may vary with application, suggestions for increasing the mechanical strength of the foam include increasing the ceramic content to 40 vol% or modifying the grain size by altering the sintering temperature. In addition, infiltration with polymer is expected to increase the compliance of the compressive

behavior and enhance the relaxation behavior of the composite, while lowering the acoustic impedance of the overall sensor. For such applications it is important to maintain a balance between mechanical properties and electrical properties of the piezocomposite. Therefore the current method of producing foams and the resulting microstructure are expected to produce an acceptable balance between the two properties, thus making it suitable for sensor applications.

4.3.2 Model Fit

The stress-strain behavior of the foams discussed here reveals an elastic response followed by an inelastic response that consists of the cell collapse in the foam. If the compressive load was continue, the foams would have exhibited a densification regime which is typical of any cellular material. This complex behavior was captured using the following phenomenological model by Liu and Subhash[36]

$$\sigma = A\frac{e^{\alpha\varepsilon}-1}{B+e^{\beta\varepsilon}} + ke^{C}(e^{\gamma\varepsilon}-1) \qquad (4\text{-}1)$$

The first term in the model captures the elastic response and the cell collapse process whereas the second term captures the densification response. However, the interest is only in the early part of the response consisting of the elastic and cell collapse regimes, as shown in Figure 4-8 and Figure 4-9. Only the first term in the above phenomenological model was used to fit these strain-strain curves.

Recently Walters et al.[37] extended the above model to both compression and tensile regimes and were able to determine several other parameters through extensive experimentation on five different density foams. The advantage of such a model is that one can determine the response of foam at intermediate densities that were not originally available. The model can also calculate tensile strength of the foam as will be describe below.

In the above equation, the parameter *A* represents the yield stress (or collapse stress) and parameter *B* represents the ratio of ultimate tensile strength to collapse stress. [37] Parameters α and β describe the plateau region of the stress-strain response. For $\alpha > \beta$, a hardening-like

behavior is observed, $\alpha = \beta$ represents the perfectly-plastic response and, $\alpha < \beta$ represents a softening-like behavior. By fitting the experimental data with the first term in the model equation, the model parameters described above (*α, A, and B*) can be obtained. The relationship between the model parameters and foam mechanical properties were determined by Walter et al. [37] as follows:

$$A \approx \sigma_C \tag{4-2}$$

$$B \approx \frac{\sigma_C}{\sigma_{ult}} \tag{4-3}$$

$$E = \frac{A\alpha}{1+B} \tag{4-4}$$

Figure 4-8 and Figure 4-9 show the comparison between the experimental data and the model fit for the LPU- and the CPU-$BaTiO_3$ foams, respectively. As shown, the model accurately captures both the elastic and plateau regions; therefore with the parameters determined from the model, the compressive modulus and collapse stress can be accurately calculated using the equations listed above.

Figure 4-10 illustrates the difference in model parameter as a function of density. The difference in trends for *α* and *β* between CPU and LPU is purely mathematical and due to the fact that the collapse stresses for CPU are under 1 MPa and the collapse stresses for LPU are above 1 MPa. This is also the reason why the values for *α* and *β* are much higher for the ceramic foams compared to *α* and *β* for the polymer foams[37]. Compared to the model parameters obtained by Subhash et al.[36] when testing polymer foams, some of the trends are different. For the ceramic foams, α and β depend on the mechanical strength of the material, *A* increases and *B* remains relatively constant with increasing density.

The values of the mechanical properties obtained from the model are comparable to the values determined previously from the measured data as seen in Figure 4-11. Clearly, the model captures the experimental data well. Therefore, the model can now be extended to other density foams with the range of densities tested here because the trends in the model

parameters are now known. We can also determine the ultimate tensile strength of these foams with the above equation. Note that, unlike the compression response where large strains are noted, brittle foams exhibit small strain in tension before failure. This extended experimental work by Walter et al.[37] has determined the relationship for structural foams.

Figure 4-12 shows the expected ultimate tensile stresses (σ_{ult}) of the ceramic foams as determined using the above equation. As expected, the tensile strength of the $BaTiO_3$ foams is significantly less than the compressive strength (three times) due to the inherent brittle behavior of ceramics. The ultimate tensile strength increases with density. Interestingly, it is noted that the tensile strength of the LPU foams increase linearly whereas the tensile strength of the CPU foams increase nonlinearly. More in-depth experimentation and model analysis is required to further validate these values in this class of ceramics.

The properties determined here provide a starting point for optimization of the foams in future studies were the ceramic foams will be infiltrated with polymeric materials for enhanced piezoelectric effect.

4.4 Conclusion

The mechanical properties of $BaTiO_3$ foams synthesized via direct foaming method using a commercial and a laboratory developed rigid, Si-free polyurethane systems were determined using confined compression testing. There was an increase in modulus and collapse strength with increasing density in both foams. The LPU foams were denser compared to the CPU foams (0.82 g/cm^3 vs. 0.51 g/cm^3), and hence had a higher modulus (6.92 MPa) and collapse strength (0.91 MPa) than the CPU foam (4.16 MPa and 0.47 MPa, respectively). The mechanical properties of LPU foam are more strongly dependent on density than CPU foams. The mechanical properties of both foams were comparable with the mechanical properties of other ceramic foams such as SiOC and Cordierite.

The phenomenological model proposed by Liu and Subhash[36] captured the elastic and plateau regions of the compressive behaviour reasonably well. The model parameters determined also compare well with the experimentally determine properties.

Based on this work, it is suggested that these ceramic foams have good mechanical properties and the potential for electromechanical applications such as piezo-sensors where they can be infiltrated with polymer to create a piezocomposite with enhanced the piezoelectric and mechanical properties.

Table 4-1. Porosity and density values for LPU foams.

Ceramic Content (vol%)	Porosity (%)		Density (g/cm^3)	
	CPU	LPU	CPU	LPU
32	87.0	80.0	0.78	1.20
31	88.0	84.7	0.72	0.92
30	91.0	85.3	0.54	0.88
29	93.0	86.3	0.42	0.82
28	93.7	92.8	0.38	0.43
Average	90.6	85.8	0.57	0.82
StDev	2.95	4.6	0.18	0.28

Table 4-2. Mechanical properties for LPU foam.

Ceramic Content (vol%)	E_C (MPa)		σ_C (MPa)	
	CPU	LPU	CPU	LPU
32	4.99	9.69	0.93	1.25
31	4.71	7.77	0.60	1.07
30	4.64	6.69	0.54	1.06
29	4.06	6.08	0.51	1.02
28	3.67	4.39	0.39	0.78
Average	4.41	6.92	0.59	0.91
StDev	0.53	1.97	0.21	0.32

Table 4-3. Properties of various ceramic foams and commercial PZT.

Parameter	$BaTiO_3$ Foam LPU	$BaTiO_3$ Foam CPU	SiOC Foam Macrocellular[38]	Cordierite Foam[39]	Bulk PZT[41]
ρ (g/cm^3)	0.43	0.42	0.4	0.34	7.6
E (MPa)	4.39	3.78	-	-	66,000
σ_c (MPa)	0.78	0.47	3.2	0.73	> 517

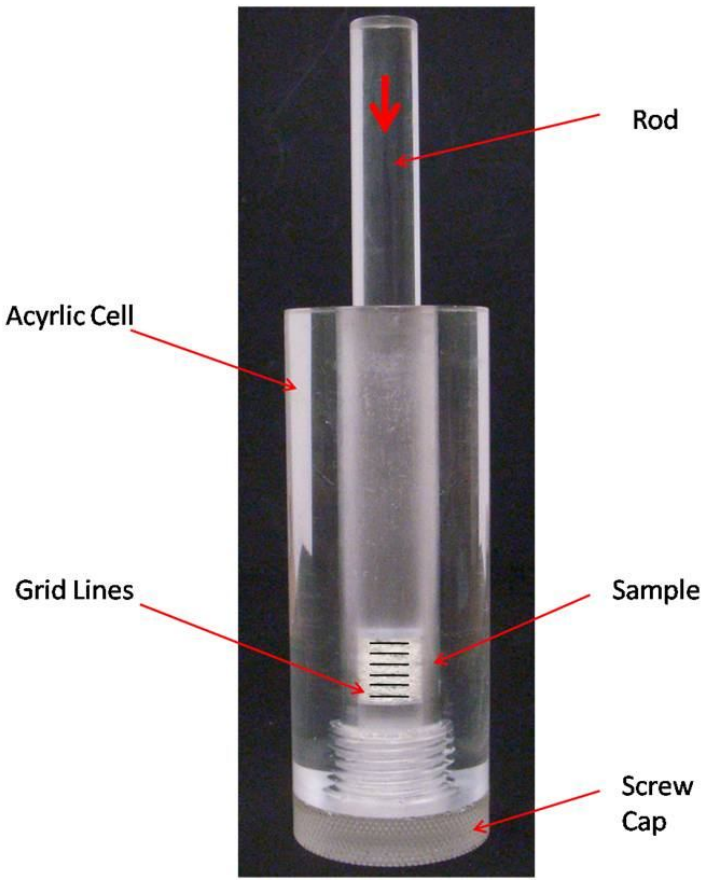

Figure 4-1. Confinement cell and foam sample used for confined compression testing.

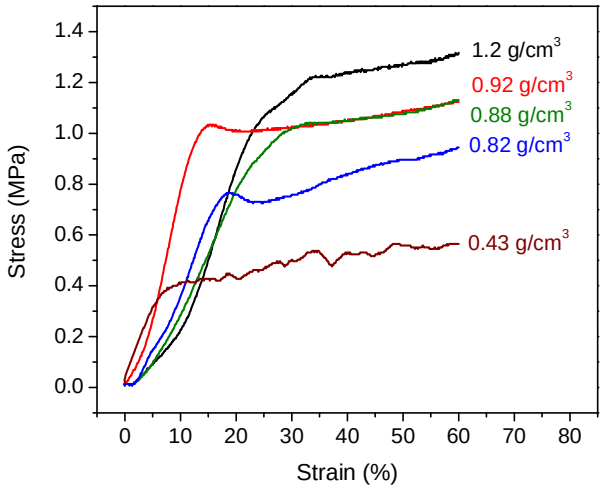

Figure 4-2. Stress-strain response of $BaTiO_3$ foam produced from LPU system.

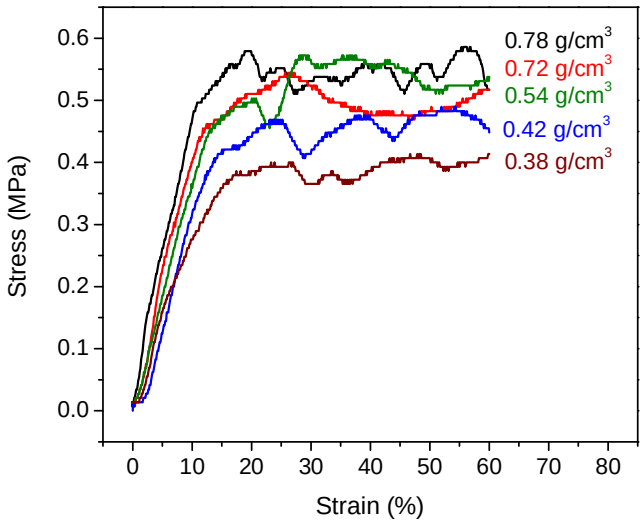

Figure 4-3. Stress-strain response of $BaTiO_3$ foam produced from CPU system.

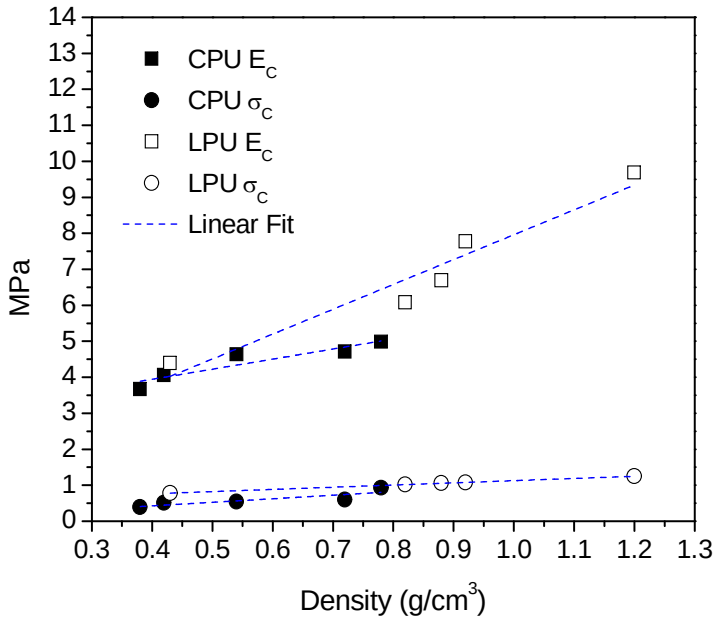

Figure 4-4. Mechanical properties of $BaTiO_3$ foam as a function of density.

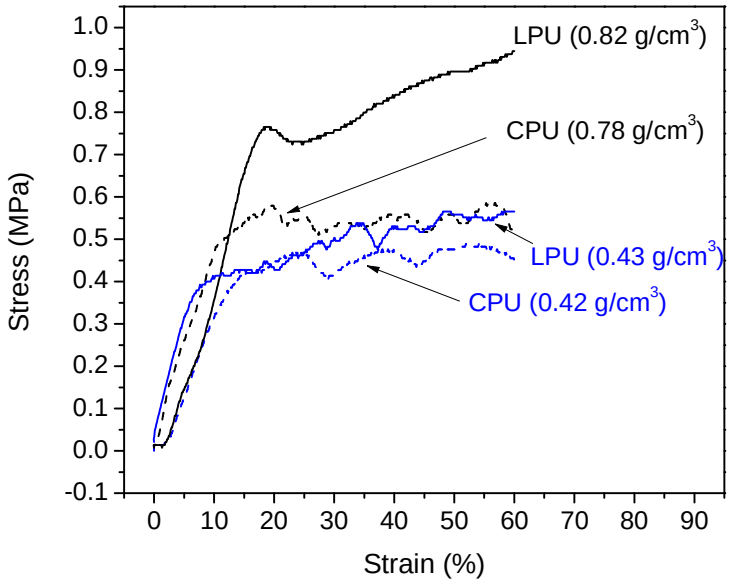

Figure 4-5. Stress-strain curves comparing density and PU.

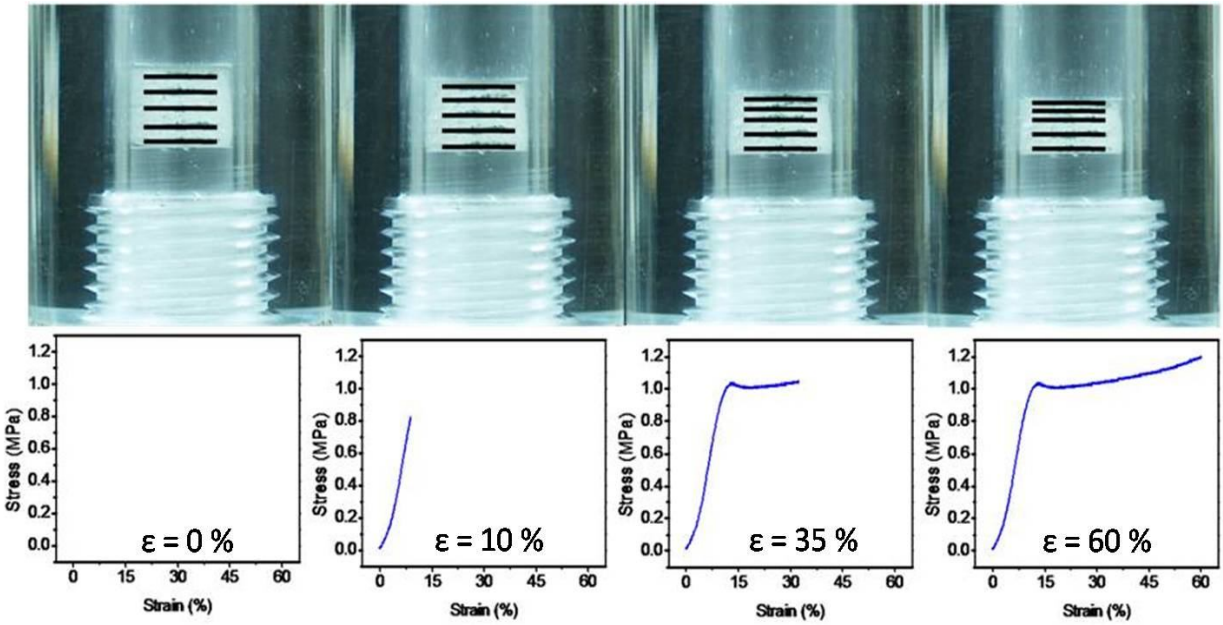

Figure 4-6. Compression of LPU foam with respective stress-strain curves.

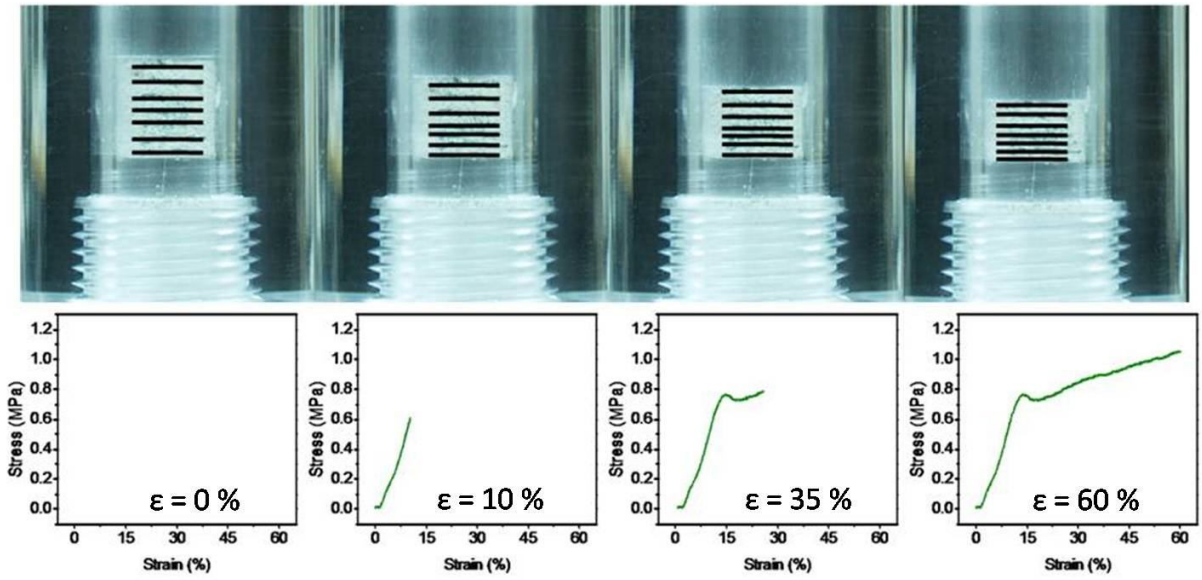

Figure 4-7. Compression of CPU foam with respective stress-strain curves.

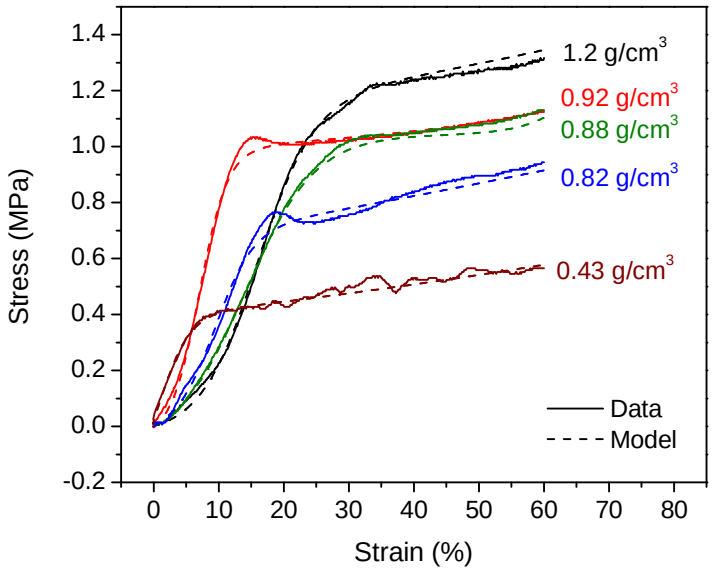

Figure 4-8. Measured data and model fit for $BaTiO_3$ foam produced by LPU.

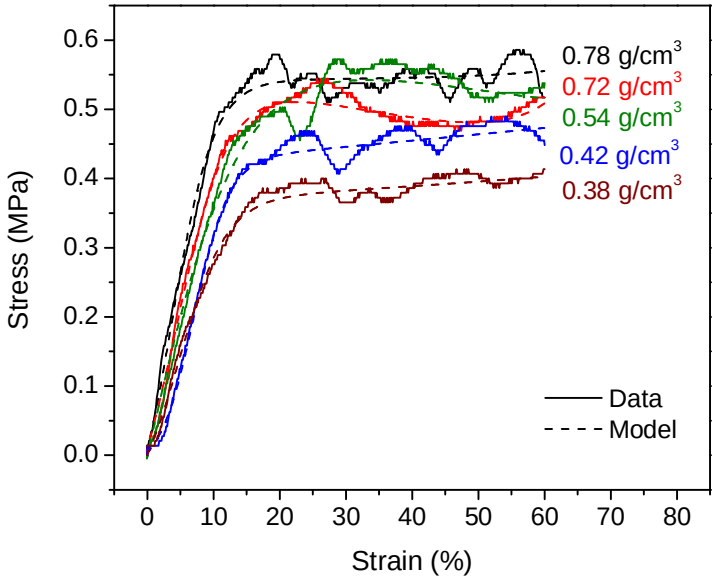

Figure 4-9. Measured data and model fit for $BaTiO_3$ foam produced by CPU.

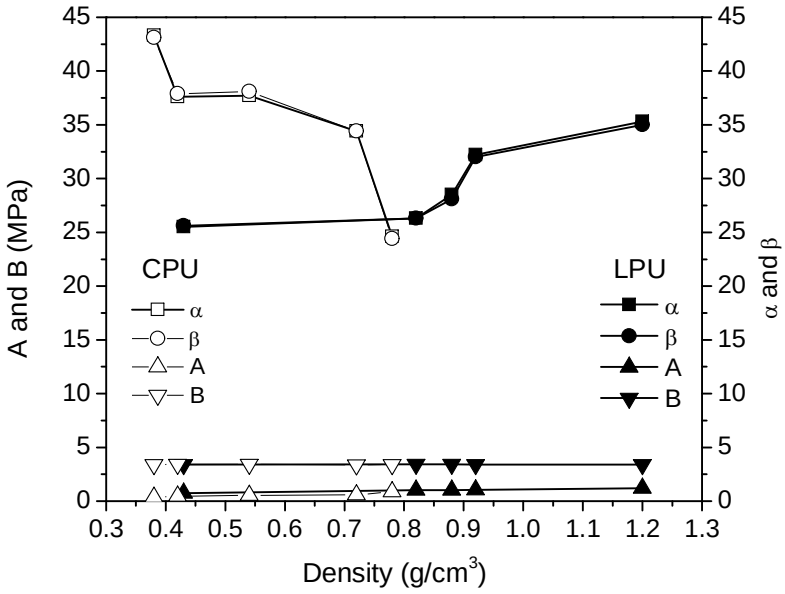

Figure 4-10. Model parameters as a function of density.

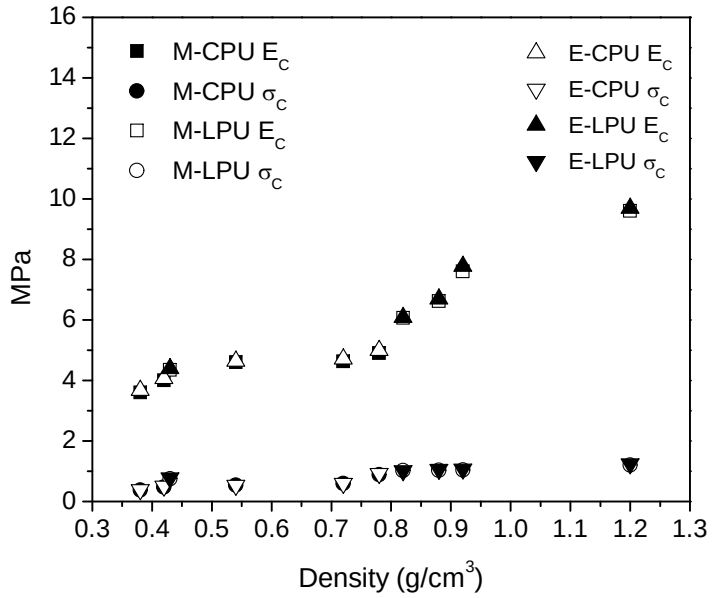

Figure 4-11. Comparison of mechanical properties determined from the (M-) fitted data and (E-) experimental data as a function of density.

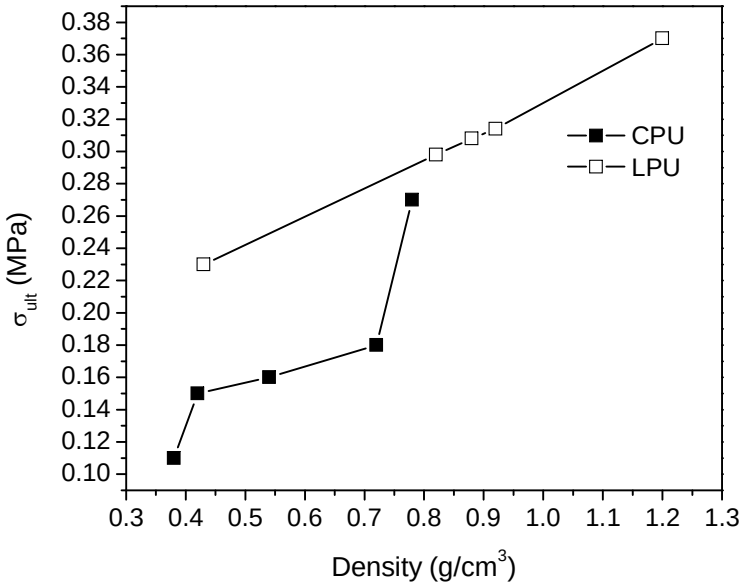

Figure 4-12. Model estimated ultimate tensile strength of $BaTiO_3$ foams as a function of density.

CHAPTER 5
POLYMER INFILTRATION AND PRELIMINARY ELECTRICAL CHARACTERIZATION

5.1 Introduction

The ultimate goal of this work is to create a 3-3 composite. Up until now, the research has been focused on creating the electroceramic skeleton from $BaTiO_3$, which can be considered a composite composed of ceramic and air. By incorporating a second phase into the cell window network of the foam, the properties can be tailored for specific applications. For ultrasound sensors, the properties required are elastic mechanical properties and high HFOM (high d_{33} and d_{31}). Since it is known that $BaTiO_3$ has a high dielectric permittivity and a low HFOM (93×10^{-15} m^2/N)[22], the polymer must have properties that will improve the properties of the composite. Although the polymer might not be piezoelectric, its high compliance allows it to transfer stress to the ceramic, enhancing piezoelectric properties overall.[20] Acoustic impedance depends on the applications. For underwater sonar sensors, the composite should have an acoustic impedance comparable to water (1.569 MRayls) and for medical ultrasound applications it should be comparable to body tissue.[4] Ceramic piezoelectrics have high acoustic impedances which differ greatly from the acoustic impedance of water while polymers have low acoustic impedances which can mediate the high difference when coupled with the ceramic.[20]

Besides polymer selection, the infiltration process is also important. A simple process that achieves complete infiltration at room temperature is desired. Vacuum assisted impregnation is that process.[17,18] Coupled with the right polymer, the 3-3 composite is achieved.

5.2 Experimental Procedure

5.2.1 Polymer Infiltration

Previously synthesized LPU foams are cut into either 8 x 8 x 5 mm plates for dielectric and piezoelectric characterization or 25.4Øx2 mm cylindrical specimens for acoustic impedance measurements. These dimensions are based on application frequency and literature. For piezoelectric measurements, the samples are cut in compliance with preferred dimensions for

optimum piezoelectric measurements.[41] The samples are then put into a polymer container and set in the vacuum chamber of the Epovac (Logitech Ltd, Glasgow, Scotland, U.K.) shown in Figure 5-1. The pressure of the chamber is lowered to 0 MPa and held for 3 minutes to ensure that all moisture has been removed from the sample. After, the polymer is poured into the polymer containing the sample very slowly. Once the sample is completely covered, pressure is raised to atmosphere and the sample is removed. After the polymer is cured, the sample is polished to remove excess polymer and vacuum grease. Scanning electron microscopy (SEM) and optical microscopy are used to characterize the composite.

5.2.2 Electrical Characterization

For electrical characterization, the plates were coated (Au/Pd) and electroded using silver paint. The capacitance and loss (tan δ) were measured as a function of frequency using a precision LCR meter connected and computer interface. From this data, the relative dielectric constant (ε_r'), also known as the real part of the permittivity, and the imaginary part of the permittivity (ε_r'') could be calculated using the equations[21]:

$$\varepsilon_r' = \frac{Ct}{\varepsilon_0 A} \tag{5-1}$$

$$\varepsilon_r'' = \varepsilon_r' \tan\delta \tag{5-2}$$

The samples were then poled in jojoba oil at 60 ^oC under an electric field of 30 kV/cm.[42] Average piezoelectric coefficients for the materials (d_{33} and d_{31}) were measured using a standard piezoelectric meter system. From these measurements the HFOM ($d_h g_h$) could be calculated and compared to the HFOM of bulk $BaTiO_3$, bulk PZT and other piezoelectric composites.

The impedance of the composite was measured to determine the resonant frequencies which can then be used to calculate the electromechanical coupling coefficients (k_{eff}, k_{33}, k_h, etc).. Resonance measurements are performed using a precision impedance analyzer. The results are discussed here.

5.3 Results and Discussion

5.3.1 Polymer Infiltration

The important properties to consider when choosing which polymer to use for infiltration are viscosity, cure time, cure temperature and hardness. Epoxies used in casting and injection molding were first considered because of their low viscosities and ability to be molded. The cure time had to be long enough so that the polymer didn't cure before completely infiltrating the sample but short enough to be practical for commercial application. In addition, a polymer that cures at room temperature makes the process simpler and prevents the structures from transitioning at higher temperatures. Finally, a low hardness and dielectric constant are desired for the piezoelectric application. Table 5-1 lists the polymers and the respective properties that were considered for infiltration taken from the company websites.

There has been previous work on composites which used the polymer polyvinyl difluoride (PVDF) because it is one of the few polymers which is piezoelectric. While this is an interesting property for piezocomposites, using PVDF to infiltrate is a difficult process because the solvent is usually a complex organic and the solution does not have a low viscosity, which is why PVDF was not chosen for the first batch of composites, but may be used later to optimize the electrical properties.

Based on the properties listed above and availability, Epofix was chosen for infiltration. In addition, it also commonly used in SEM to increase contrast. The resulting SEM images of the composite are shown in Figure 5-2. From these images, it can be seen that the foam system has been completely infiltrated and that the ceramic foam is a homogeneous phase. Unfortunately, the SEM image cannot show the 3-3 connectivity of the composite since it is a 2-dimensional technique. While it can be assumed that the composite has 3-3 connectivity because the foam originally had 3-3 connectivity between the foam and air, another characterization technique will need to be used in order to create 3-dimensional images of the

composite. Regardless, a 3-3 composite has been achieved between ceramic foam and polymer.

5.3.2 Electrical Characterization

Figure 5-3 shows the capacitance and loss of the composite as a function of frequency from 40 Hz to 110 MHz, respectively. Using the equation mentioned above, the dielectric permittivity of the material is calculated and also shown as a function of frequency from 40 Hz to 110 MHz in Figure 5-4. The typical frequency range for ultrasound applications is above human hearing which is 20 kHz.[4] As seen from the figure, the dielectric constant decreases with increasing frequency. Therefore, for ultrasound applications the piezoelectric properties increase due to the decreasing dielectric constant.

Table 5-2 lists the piezoelectric coefficients including d_{33}, d_{31}, and $d_h g_h$ for the composite. It is assumed that $\varepsilon_r \sim \varepsilon_r'$. The static dielectric constant (at 1 kHz) was used to calculate the HFOM. The theoretical static dielectric constant was calculated using the rule of mixtures, assuming the volume fraction of ceramic is about 7 vol%, and compared to the experimental value. This value is 144.6, which is similar to value determined experimentally. The term ε_{33} in the HFOM equation is the dielectric constant multiplied by the permittivity of free space.

From the measurements and calculations, the piezocomposite has a lower HFOM than bulk $BaTiO_3$ and bulk PZT. This is could be due to a couple of factors. Firstly, the volume of fraction of piezoelectric material is only about 10 vol%. An increase in the HFOM is expected with an increase in the amount of piezoelectric material in the ceramic. A theoretical HFOM as a function of volume fraction has shown in Figure 5-5. It is observed that the HFOM peaks at about 10 vol% and that the theoretical HFOM is much higher than the measured HFOM at 7 vol%. This is most likely due to the poling conditions. The polymer limits the temperature and electric field that can be used to pole the composite. However, the focus of this work was to successfully create a 3-3 composite and measure the piezoelectric properties, which has been

achieved. The next step is to improve these properties further through material selection, using piezoelectric materials such as PZT and PVDF as mentioned above.

The impedance of the composite was measured; however no resonant frequencies were observed indicating that the composite acted like a capacitor. This is due again to the choice of materials and to the low ceramic volume fraction in the composite which would be the source of the resonance. Future work consists of attempting these measurements again with a higher ceramic content composite made of PZT.

5.4 Conclusion

Using $BaTiO_3$ foam synthesized via direct foaming method as discussed in previous chapters, a composite was fabricated which has 3-3 connectivity. Different polymers were considered for infiltration based on their viscosity, cure time, cure temperature, hardness and dielectric constant. The purpose of the polymer in the composite is to decrease the dielectric constant, acoustic impedance and brittle behavior of the foam while enhancing the HFOM. Based on these properties, Epofix resin commonly used for mounting samples for SEM characterization due to its high phase contrast was chosen.

The samples were infiltrated using Epovac equipment which is a vacuum impregnation system. Using this technique, polymer infiltrated all empty space in the foam. Using SEM, it was confirmed that the foam was completely infiltrated, creating a 3-3 composite with the ceramic foam. However, only a 2D image could be taken using this technique. Therefore, a 3D image will be achieved later to show the interconnecting phases.

After the composite was fabricated, preliminary electrical characterization measured the piezoelectric and dielectric properties of the material. After the samples were poled at 60 ^{o}C for 30 minutes under a 30 kV/cm field, the piezoelectric coefficients (d_{33}, d_{31} and $d_h g_h$) were measured using a piezoelectric meter. The HFOM of the composite (53.7 x 10^{-15} m^2/N) did not exceed the HFOM of bulk $BaTiO_3$ or bulk PZT. This is due to the low compliance of the polymer chosen for infiltration and this knowledge will be used in determining a different polymer for the

composite in the next experiments. This is also due to the low volume fraction of piezoelectric material in composite. In addition, resonance measurements were unsuccessful since resonance was not observed in the composite again due to the material choice and low ceramic content. However, the 3-3 piezoelectric composite has been successfully fabricated. Now, the composite can be fabricated with better piezoelectric materials such as PZT and PVDF, using the processes developed in this work.

Table 5-1. Material properties of polymers considered for infiltration.

Polymer	Viscosity (cps)	Hardness	Cure Time (h)	Cure Temperature	Dielectric Constant
EP5340 (Eager Polymers)	600	88D	24	25 ^{o}C	4.57
PVDF (Kynar)	3.1E6	78D	-	-	~ 10
Epofix (Struers)	50	75D	8	25 ^{o}C	~ 5

Table 5-2. Piezoelectric coefficients of composite and bulk materials.

Material	ρ (kg/m^3)	ε_r'	d_{33} (pC/N)	d_{31} (pC/N)	$d_h g_h$ (10^{-15} m^2/N)
$BaTiO_3$ piezocomposite	1737	156	45	-18	58.7
Bulk $BaTiO_3$[19]	6200	1400	190	-78	93
Bulk PZT-8[41]	7600	-	225	-27	100

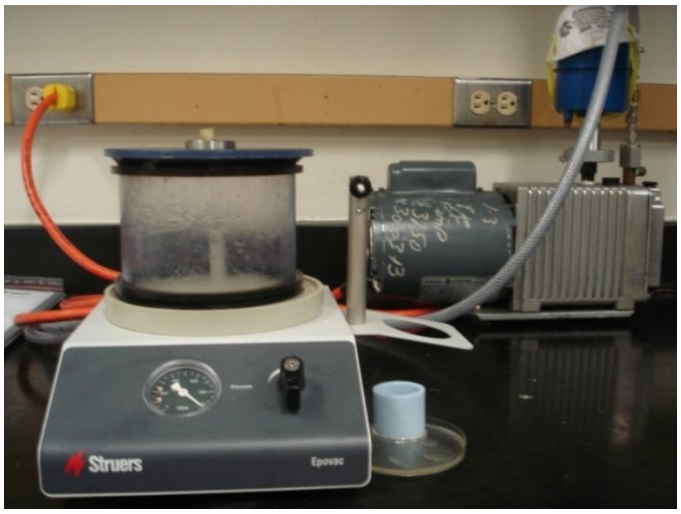

Figure 5-1. Epovac system for polymer impregnation.

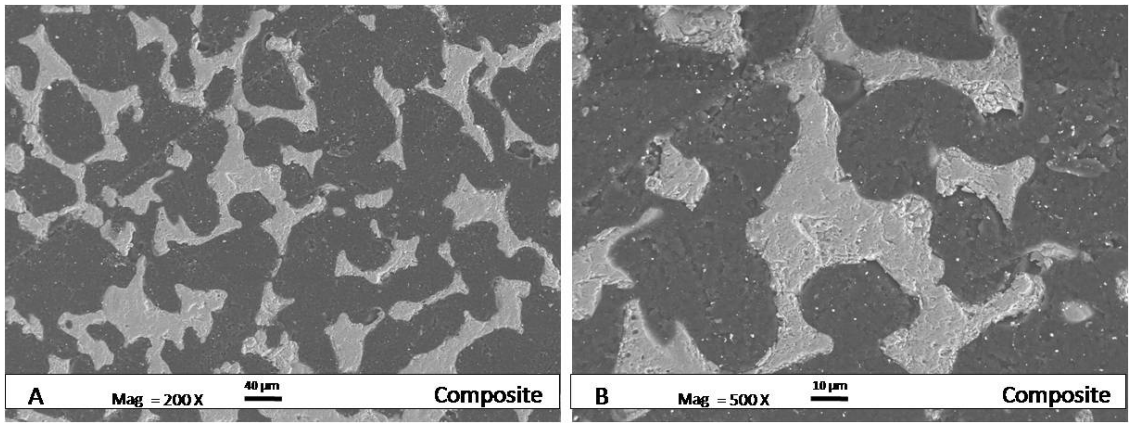

Figure 5-2. SEM images of the infiltrated composite: (light) $BaTiO_3$, (dark) Epofix.

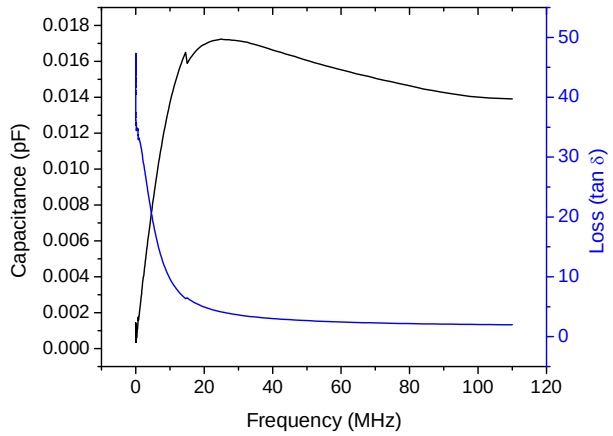

Figure 5-3. Capacitance and loss of composite as a function of frequency.

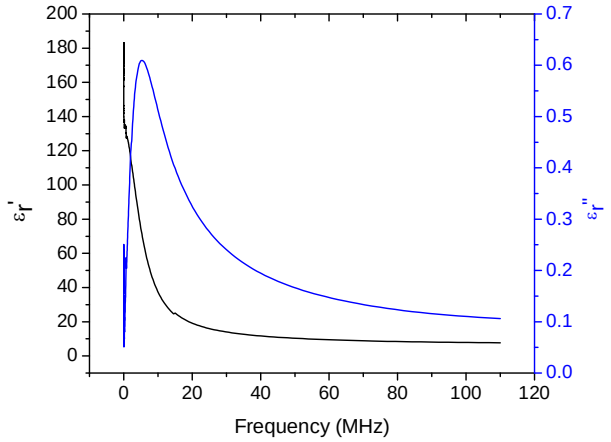

Figure 5-4. Permittivity (real and imaginary) of composite.

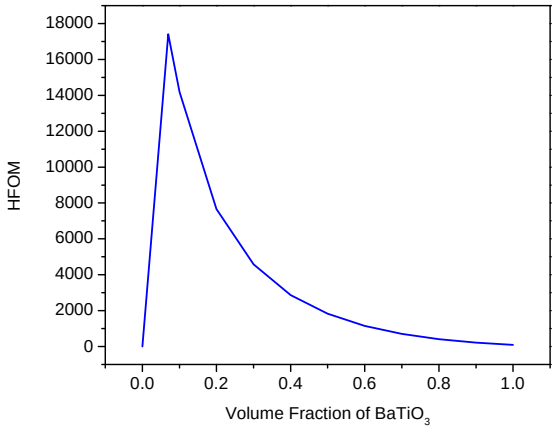

Figure 5-5. Theoretical HFOM as a function of ceramic volume fraction.

CHAPTER 6
SUMMARY AND OUTLOOK

6.1 Summary

A surfactant-stabilized direct foaming method was used to create $BaTiO_3$-based ceramic foams. The composition, polyurethane system and sintering time were varied to determine their influence on the microstructure of the foam and ultimately the properties and applications of the foam. After determining that Si-based PU systems produced contaminants at the grain boundary and inhomogeneous grain size distributions and flexible PU systems produced closed cell structures, research was focused on Si-free, rigid PU systems: one commercially purchased and the other laboratory developed. After additional initial testing, some of the other variables were eliminated. The primary synthesis variables were polyurethane system (CPU – commercial and LPU – laboratory) and composition (20 – 60 vol% ceramic).

Both the rigid commercial and rigid laboratory systems produced foams with uniform cell window size distributions and dense, thick struts. However, the commercial system's struts consisted of many small grains, while the laboratory system struts had fewer but larger grains. The rigid laboratory developed system demonstrated uniform cell window distribution, variable porosity in relation to ceramic composition (75 - 87 %), dense struts, contaminant-free grain boundaries at concentrations less that 50 vol% and mechanical integrity. The commercial silicon-free system also had a uniform cell window size distribution, smaller grain size, larger cell window size and also demonstrated dense struts and variable porosity in relation to ceramic composition (82 – 93 %).

Lower ceramic concentrations (20, 30 and 40 vol%) are ideal for electrical applications because of the interconnected cell window network and increased porosity. However, they are more brittle than foams with higher ceramic concentrations (50 and 60 vol%) which are more favored in mechanical applications. 30 vol% foams demonstrated a homogeneous microstructure with a balance of properties for both mechanical and electrical applications. They

have high porosity (~ 88 %), uniform and smaller grain size, are relatively strong and not easily damaged. Raman spectroscopy indicated that compressive residual stress was created in the structure during the foaming process which could have affected the mechanical properties. This was observed by the shifts in the Raman modes of the spectra in comparison to bulk barium titanate.

A 30 vol% foam, synthesized using the laboratory developed rigid polyurethane system and a 30 vol% commercial silicon-free system, sintered for 8 hours at 1400 °C, produced different microstructures which have the potential to be used in electromechanical applications.

The mechanical properties of $BaTiO_3$ foams synthesized via direct foaming method using a commercial and a laboratory developed rigid, Si-free polyurethane systems were determined using confined compression testing. There was an increase in modulus and collapse strength with increasing density in both foams. The LPU foams were denser compared to the CPU foams (0.82 g/cm^3 vs. 0.51 g/cm^3), and hence had a higher modulus (6.92 MPa) and collapse strength (0.91 MPa) than the CPU foam (4.16 MPa and 0.47 MPa, respectively). The mechanical properties of LPU foam are more strongly dependent on density than CPU foams. The mechanical properties of both foams were comparable with the mechanical properties of other ceramic foams such as SiOC and Cordierite. The properties determined here provide a starting point for optimization of the foams in future studies were the ceramic foams will be infiltrated with polymeric materials for enhanced piezoelectric effect.

The phenomenological model proposed by Liu and Subhash[36] captured the elastic and plateau regions of the compressive behaviour reasonably well. Using this model, the properties and stress-strain behaviour of intermediate densities can be calculated without being measured. These properties include compressive modulus (E_C), collapse stress (σ_C) and the ultimate tensile stress (σ_{ult}). The properties determined by the experimental data and the properties determined by the model were very similar, which verified the model's capabilities to accurately determine the mechanical properties of the ceramic foam.

Finally, using $BaTiO_3$ foam, a composite was fabricated which has 3-3 connectivity. Different polymers were considered for infiltration based on their viscosity, cure time, cure temperature, hardness and dielectric constant. The purpose of the polymer in the composite is to decrease the dielectric constant, acoustic impedance and brittle behavior of the foam while enhancing the HFOM. Based on these properties, Epofix epoxy commonly used for mounting samples for SEM characterization due to its high phase contrast was chosen.

The samples were infiltrated using Epovac equipment which is a vacuum impregnation system that successfully infiltrated all empty space in the foam. Using SEM, it was determined that the foam was completely infiltrated, creating a 3-3 composite with the ceramic foam. However, only a 2D image could be taken using this technique. Therefore, a 3D image will be achieved later to show the interconnecting phases.

After the composite was fabricated, preliminary electrical characterization measured the piezoelectric and dielectric properties of the material. After the samples were poled at 60 ^oC for 30 minutes under a 30 kV/cm field, the piezoelectric coefficients (d_{33}, d_{31} and $d_h g_h$) were measured using a piezoelectric meter. The HFOM of the composite (53.7 x 10^{-15} m^2/N) did not exceed the HFOM of bulk $BaTiO_3$ or bulk PZT. This is due to the low compliance of the polymer chosen for infiltration and this knowledge will be used in determining a different polymer for the composite in the next experiments. The experimental HFOM is lower than the calculated theoretical HFOM. However, the 3-3 piezoelectric composite has been successfully fabricated. Now, the composite can be fabricated with better piezoelectric materials such as PZT and PVDF, using the processes developed in this work. In addition, resonance measurements were unsuccessful since resonance was not observed due to the material choice and low ceramic volume fraction. Now, the composite can be fabricated with better piezoelectric materials such as PZT and PVDF, using the processes developed in this work.

6.2 Outlook

While there have been many accomplishments achieved in this work including a unique electroceramic foam structure and 3-3 piezocomposites, there is still a lot of research to do in order to optimize and fully characterize the 3-3 piezocomposite. These include synthesizing composites with higher piezoelectric material volume fraction, resonance measurements, acoustic impedance measurements and composite structure characterization using a 3D imaging technique such as TEM. In addition, characterization of the composite mechanical properties and eventually the optimization of the mechanical properties and electrical properties should be achieved in the future.

The acoustic impedance of the composite is measured using equipment consisting of a speaker, wave guide and sample holder. The samples are cut into a 25.4 mm diameter cylinder, mounted onto the sample holder, and placed at the end of the wave guide. The acoustic impedance is measured at 20 kHz to simulate ultrasound conditions. The measured acoustic impedance is then compared to the acoustic impedance of water and tissue to determine if it had acceptable properties of ultrasonic sensor applications either underwater or in medicine. Additionally, the effective acoustic piezoelectric modulus will be measured using the same samples from the acoustic impedance measurements. The samples are poled and vibrated using a laser-vibrometer.

As stated in Chapter 5, an additional imaging technique is desired to characterize the composite structure because SEM can only show that the phases are interconnected in two dimensions, while this work is focused on achieving connectivity in 3 dimensions. In addition, there has been work by Wachsman et al. on quantifying 3-3 connectivity. In most cases, connectivity is characterized by imaging techniques and is only qualitative. However, this new work has been able to quantify this property by creating relationships between the number of nodes and struts in either phase of the composite.

As stated previously, there has been little research on the required (minimum) mechanical properties of piezoelectrics. Future work will determine this by characterizing the compressive and relaxation behavior of the composites. In addition, the piezocomposite structure will be optimized to enhance mechanical properties and electrical properties. This includes using different materials for the composite such as PZT and PVDF to observe their effect on the HFOM. Now that the 3-3 composite has been fabricated, the freedom to experiment with other materials for different applications is available.

APPENDIX A
IMAGE ANALYSIS

The steps used to perform image analysis on the FE-SEM images of the foams made by the author are described in this appendix.

1. Micrographs were taken at 1000X magnification and different locations on the sample. The images used did not have scale bars or labels on them. This prevents the software from calculating the label which would affect the data output.

2. Using an image editing software, such as Photoshop, the grain boundaries are digitally enhanced to increase contrast in the image as shown in Figure A-1.

3. Image J software is opened and the image is opened in the program.

4. Image>Type>32-bit. This changes the image from an RGB image to a 32-bit image. If the image is not converted, it cannot be analyzed.

5. Image>Adjust>Brightness/Contrast. The contrast is adjusted to the extreme so that the grains are white and grain boundaries and cell windows are black as shown in the Figure A-2 below.

6. Adjust>Threshold. Adjust the threshold so that the feature to be measured is red. For example, if the grain size is being measured, then the grains should be red. Images for both grain size measurements and cell window size measurements are shown in Figure A-3.

7. Analyze>Analyze Particles. As stated in Chapter 3, the macro then calculates the number of red pixels and then prints out the results and summary of the calculation which include the average area.

8. Because the macro reports the area of the feature, the size of the feature must be determined assuming that the grains and pores are circular. As seen from the above figures, this is not the case and this method gives only an estimation of the feature sizes.

9. Based on the scale bar and magnification, the feature sizes which are calculated in pixels/feature are then converted to microns/feature which is the actual feature size.

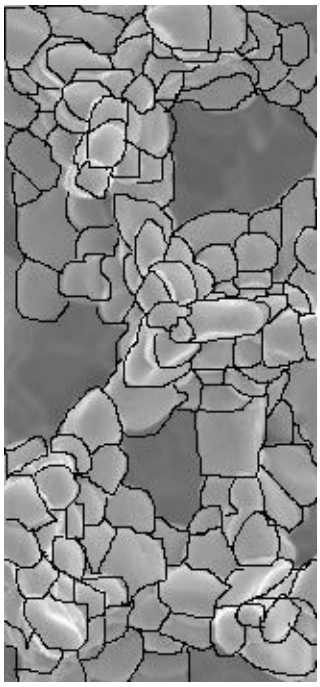

Figure A-1. Micrograph of PU2 foam with the grain boundaries digitally enhanced.

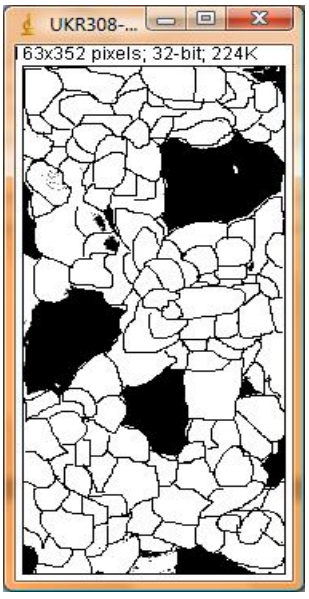

Figure A-2. Micrograph with enhanced contrast.

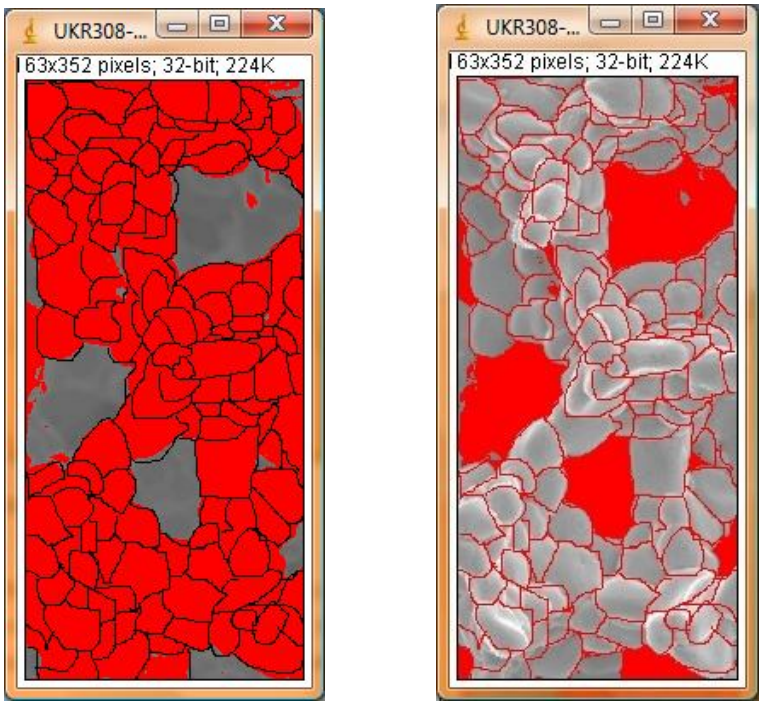

Figure A-3. Micrographs with the threshold adjusted to measure (left) grain size and (right) cell window size.

APPENDIX B
RAMAN SPECTROSCOPY

Raman spectroscopy was performed on the foam synthesized via direct foaming. This was done to determine if residual stress had formed in the structure during the foaming process. Measurements were taken at room temperature, 100 ^{o}C, and 150 ^{o}C to capture the phase transition from cubic to tetragonal at around 130 ^{o}C. The measured spectra were then compared to the Raman spectra of bulk $BaTiO_3$ pellets to determine if there were shifts in the peak center which would indicate residual stress. Table B-1 and
Table B-2 are the character tables for cubic and tetragonal barium titanate, respectively, based on group theory. The high temperature cubic phase has no Raman active modes while the lower temperature tetragonal phase has seven Raman active modes and six infrared active modes.

All measurements were taken using a Reinshaw Biotherm Raman microscope and temperature controlled sample holder. The experiments were part of a collaboration with Professor Ian Reaney and Dr. Honza Pokorny at the University of Sheffield.

Figure B-1 is the measured Raman spectra. It is observed that due to background noise, nine modes were required to fit the data. While group theory estimates that there are no Raman active modes in the cubic phase, it is not uncommon to see tetragonal phase peaks in the supposedly cubic structure. This is due to local tetragonal phases at the atomic level which are detected in the Raman spectroscopy.

Figure B-2 shows the Raman spectra and change in peak center between the pellet and foam as a function of peaknumber for each temperature. The major modes to notice are peak numbers 3, 6, 7 and 9 as they are prominent peaks in the spectra. According to Figure B-2 there is a significant difference in the peak centers of 6, 7 and 9 at 150 ^{o}C between bulk barium titanate and the foam. This indicates that there is residual stress formed during the foaming process, creating tensile stresses which cause the bonds to stretch and tighten thus vibrating at higher frequencies. Interestingly, peak number 3 does not appear in the foam at 150 ^{o}C.

Table B-1. Character table for ABO_3 cubic structure

	Distribution of Degrees of Freedom		Number of normal modes			
O_h	A and B cations O_h 1(a), 1(b)	O anion D_{4h} 3(c)	Acoustic Modes	Rotational Modes	Lattice Modes	Selection Rules
A_{1g}	0	0	0	0	0	Raman
A_{1u}	0	0	0	0	0	Inactive
A_{2g}	0	0	0	0	0	Inactive
A_{2u}	0	0	0	0	0	Inactive
E_g	0	0	0	0	0	Raman
E_u	0	0	0	0	0	Inactive
F_{1g}	0	0	0	1	0	Inactive
F_{1u}	2	2	1	0	3	Infrared
F_{2g}	0	0	0	0	0	Raman
F_{2u}	0	1	0	0	1	Inactive

$$\Gamma = 3F_{1u}(IR)$$

Table B-2. Character table for ABO_3 tetragonal structure

	Distribution of Degrees of Freedom		Number of normal modes			
C_{4v}	A, B, and O_1 C_{4v} 1(a), 1(b)	O_2 C_{2v}^{v} 2(c)	Acoustic Modes	Rotational Modes	Lattice Modes	Selection Rules
A_1	3	1	1	0	3	Raman and Infrared
A_2	0	0	0	1	0	Inactive
B_1	0	1	0	0	1	Raman
B_2	0	0	0	0	0	Raman
E	3	2	1	1	3	Raman and Infrared

$$\Gamma = 3A_1(R,IR) + B_1(R) + 3E(R,IR)$$

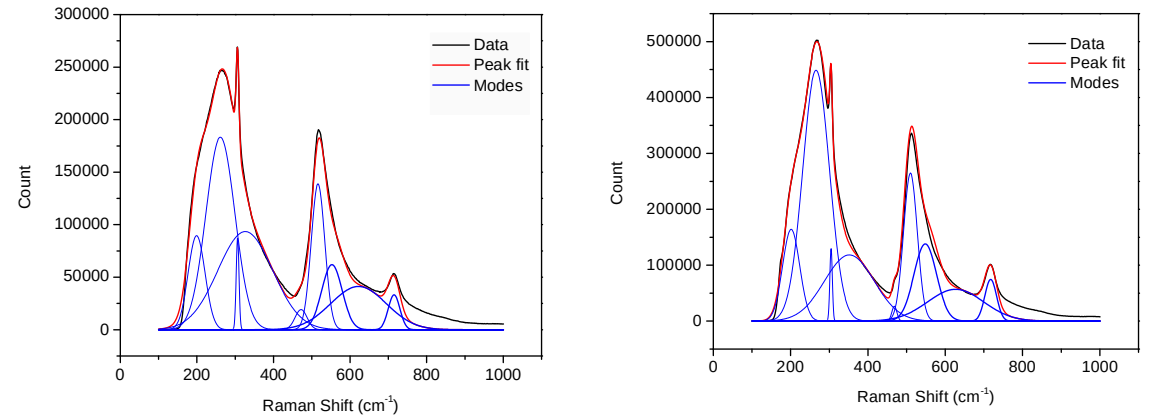

30 °C

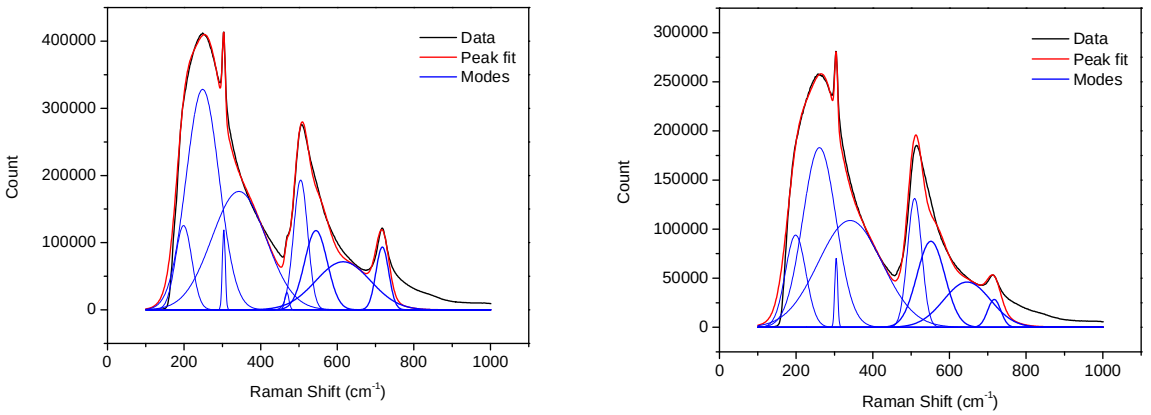

100 °C

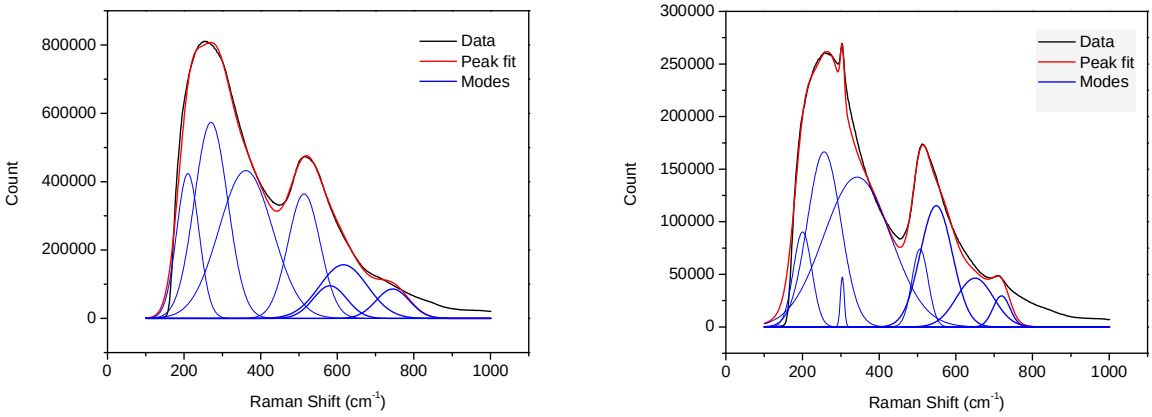

150 °C

Figure B-1. Raman spectra of (left) bulk barium titanate and (right) barium titanate at different temperatures.

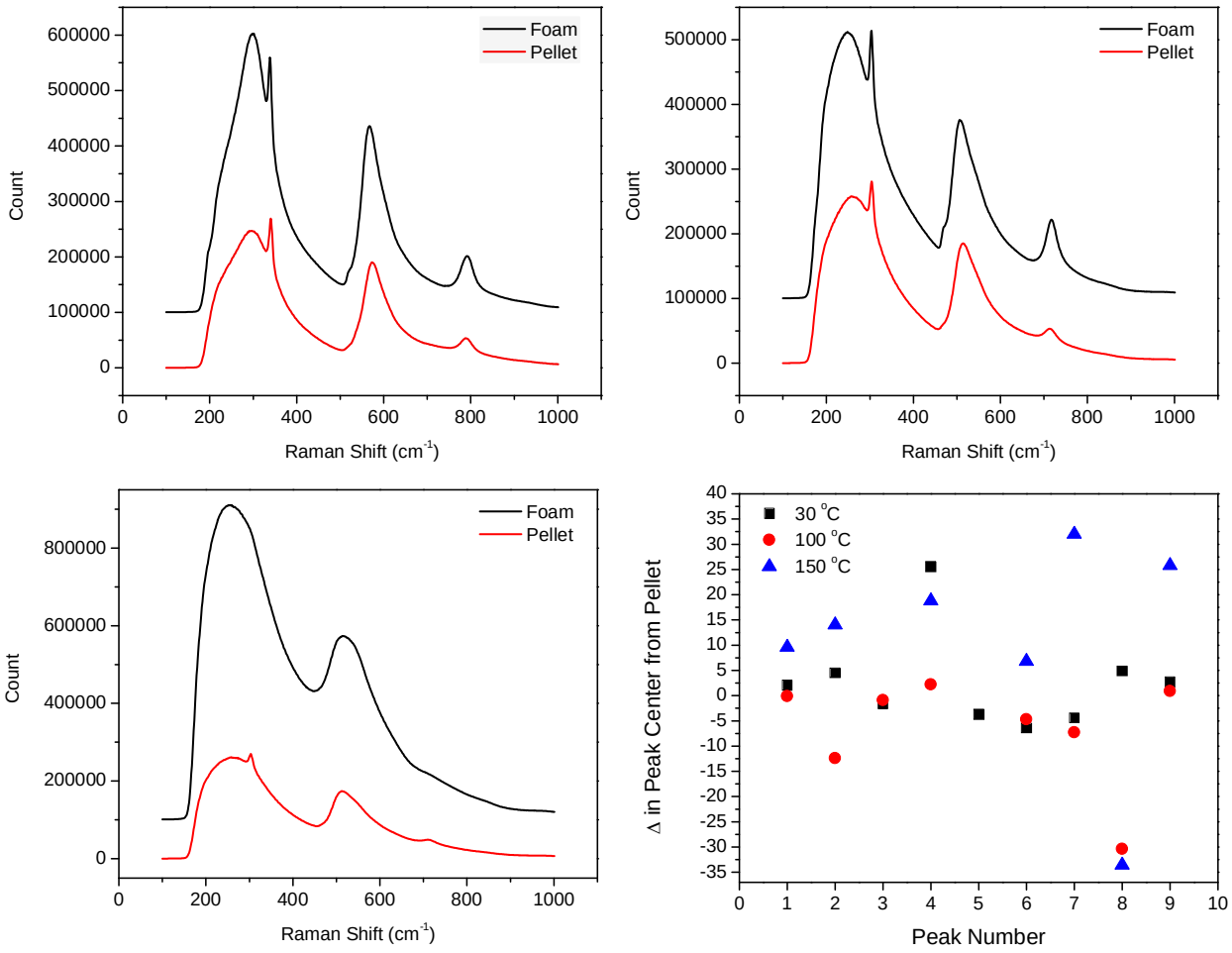

Figure B- 2. Raman spectra comparison between barium titanate foam and pellet (top left) at 30 °C, (top right) at 100 °C and (bottom left) 150 °C and the difference in peak center (foam peak center – pellet peak center).

REFERENCES

1. R.E. Newnham, D.P. Skinner and L.E. Cross, “Connectivity and Piezoelectric-Pyroelectric Composites”, *Mater. Res. Bull.,* **13** [5] 525-536 (1978).

2. M.J. Haun, P.Moses, T.R. Gururaja, W.A. Schulze and R.E. Newnham, “Transversely Reinfoced 1-3 and 1-3-0 Piezoelectric Composites”, *Ferroelectrics,* **49** [1] 259-264 (1983).

3. M.J. Haun, R.E. Newnham, ”An Experimental and Theoretical Study of 1-3 and 1-3-0 Piezoelectric PZT-Polymer Composites for Hydrophone Applications”, *Ferroelectrics,* **68** [1] 123-139 (1986).

4. W.A. Smith, A.A. Shaulov, and B.A. Auld, ”Design of Piezocomposites for Ultrasonic Transducers”, *Ferroelectrics,* **91** [1] 155-162 (1989).

5. W.A. Smith and B.A. Auld, “Modeling 1-3 Composite Piezolelectrics – Thickness-Mode Oscillations”, *IEEE T Ultrason. Ferr.,* **38** [1] 40-47 (1991).

6. W.A. Smith, “Modeling 1-3 Composite Piezoelectrics – Hydrostatic Response”, *IEEE T Ultrason. Ferr.,* **40** [1] 41-49 (1993).

7. W.A. Smith, “Composite Piezoelectrics Utilizing a Negative Poisson Ratio Polymer”, United States Patent 5,334,903 (1994).

8. D.P. Skinner, R.E. Newnham, and L.E. Cross, “Flexible Composite Transducers”, *Mater. Res. Bull.,* **13** [6] 599-607 (1978).

9. T.R. Shrout, W.A. Schulze, and J.V. Biggers, “Simplified Fabrication of PZT-Polymer Composites”, *Mater. Res. Bull.,* **14** 1553-1559 (1979).

10. K. Rittenmyer, T. Shrout, W.A. Schulze, and R.E. Newnham, “Piezoelectric 3-3 Composites”, *Ferroelectrics,* **41** [1] 323-329 (1982).

11. K. Schwartzwalder, H. Somers, and A.V. Somers, “Method of Making Porous Ceramic Articles,” United States Patent 3,090,094 (1963).

12. L.J. Gauckler, A.R. Studer, U.T. Gonzenbach, E. Tervoort, “Processing Routes to Macroporous Ceramics: A Review”, *J. Am. Ceram. Soc.,* **89** [6] 1771-1789 (2006).

13. P. Colombo and M. Modesti, “Silicon Oxycarbide Foams from a Silicone Preceramic Polymer and Polyurethane”, *J. Sol-Gel Sci. Techn.,* **14** [3] 103-111 (1999).

14. R. Ramesh, H. Kara, and C.R. Bowen, “Finite Element Modeling of Dense and Porous Piezoceramic Disc Hydrophones”, *Ultrasonics,* **43** [3] 173-181 (2005).

15. J.J.C. Busfield, J.R.G. Evans, Z. Fan, H.X. Peng. “Microstructure of Ceramic Foams”. *J. Eur. Ceram. Soc.,* **20** [7] 807-813 (2000).

16. Q. Liu, G. Subhash, "A Phenomenological Constitutive Model for Foams under Large Deformations", *Poly. Eng. and Sci.,* **44** [3] 463-473 (2004).

17. E. Ozcivici and R.P. Singh, “Fabrication and Characterization of Ceramic Foams Based on Silicon Carbide Matrix and Hollows Alumina-Silicate Spheres”, *J. Am. Ceram. Soc.,* **88** [12] 3338-3345 (2005).

18. G.J. Qi, C.R. Zhang, H.F. Hu, F. Cao, S.Q. Wang, Y.B. Cao, and Y.G. Jiang, “Preparation of Three-Dimensional Silica Fiber Reinforced Silicon Nitride Composites Using Perhydropolysilazane as Precursor”, *Mater. Lett.,* **59** [26] 3256-3258 (2005).

19. S. Roberts, “Dielectric and Piezoelectric Properties of Barium Titanate”, *Phys. Rev.* **71** [12] 890-895 (1947).

20. B. Jaffe, R.S. Roth, and S. Marzullo, “Piezoelectric Properties of Lead Zirconate-Lead Titanate Solid-Solution Ceramics”, *J. Appl. Phys.,* **25** [6] 809-810 (1954).

21. A.J. Moulson, J.M. Herbert, *Electroceramics*, 2nd Ed. John Wiley & Sons Ltd. (2003).

22. L.E. Cross, “Ferroelectric Ceramics: Tailoring Properties for Specific Applications”, *Ferroelectric Ceramics,* Ed N Setter and E L Colla (1993).

23. T.R. Gururaja, A. Safari, R.E. Newnham and L.E. Cross, “Piezoelectric Ceramic-Polymer Composites for Transducer Applications,” *Electronic Ceramics*, edited by L.M. Levinson, 92-128 (2004).

24. D.J. Green, and P. Colombo, “Cellular Ceramics: Intriguing Structures, Novel Properties and Innovative Applications,” *Mater. Res. Bull.,* **28** [4] 296-300 (2003).

25. P. Colombo and J.R. Hellman, “Ceramic Foams from Preceramic Polymers”, *Mater. Res. Innov.,* **6** [5-6] 260-272 (2006).

26. D.M. Liu, “Influence of Porosity and Pore Size on the Compressive Strength of Porous Hydroxyapatite Ceramic”, *Ceram. Int.,* **23** [2] 135-139 (1997).

27. X. Bao, M.R. Nangrejo, and M.J. Edirisinghe, “Preparation of Silicon Carbide Foams Using Polymer Precursor Solutions”, *J. Mater. Sci.,* **35** [17] 4365-4372 (2000).

28. P. Colombo and E. Bernardo, “Macro- and Micro-cellular Porous Ceramics from Preceramic Polymers”, *Compos. Sci. Techno.,* **63** [16] 2353-2359 (2003).

29. A. Rainer, F. Basoli, S. Licoccia, and E. Traversa “Foaming of Filled Polyurethanes for Fabrication of Porous Anode Supports for IT-SOFC” *J. Am. Ceram. Soc.,* **89** [6] 1795–1800 (2006).

30. D. Weaire, *The Kelvin Problem: Foam Structure of Minimal Surface Area*, CRC Press. (1996).

31. R.M. Stroud, J.W. Long, J.J. Pietron, E.M. Lucas, M.L. Anderson, K.E. Swyder Lyons, C.I. Merzbacher, D.R. Rolison. “Mesoporous, Microporous and Nanowired: Electron Microscopy of Aerogel Composites”, *Microsc. Microanal.,* **8** [2] 324-328 (2002).

32. X.Y. Deng, X.H. Wang, Z.L. Gui, L.T. Li and I.W. Chen, “Grain-Size Effects on the Hardness of Nanograin $BaTiO_3$ Ceramics”, *J. Electroceram.,* **10** 44-47 (2007).

33. R.W., Siegel, G.E. Fougere, “Mechanical Properties of Nanophase Materials”, NATO Conference, Corfu, Greece, 20 Jun – 2 Jul (1993).

34. L. Wucherer, J. C. Nino, F. Basoli, E. Traversa, “Synthesis and Characterization of $BaTiO_3$-based Foams with Controlled Microstructure” *Int. J. Appl. Ceram. Tech.* (In press 2008).

35. W.A. Smith and B.A. Auld, “Modeling 1-3 Composite Piezoelectrics: Hydrostatic Response”, *Ultra. Ferro. IEEE,* **40** [1] 40-47 (1991).

36. G. Subhash, Q. Liu, X.-L Gao, "Quasistatic and High Strain Rate Uniaxial Compressive Response of Polymeric Structural Foams," *Int. J. Impact. Eng.,* **32** [7] 1113-1126 (2006).

37. T.R. Walter, A. Richards and G. Subhash, “A Unified Phenomenological Model for Compression and Tension Response of Polymeric Foams,” *ASME J. of Eng. Mater. and Tech.* (in press 2008).

38. P. Colombo, J.R. Hellmann and D.L Shelleman, “Mechanical Properties of Silicon Oxycarbide Ceramic Foams,” *Comp. Sci. Tech.,* **84** [10] 2245-2251 (2001).

39. F.A. Costa Oliveria, S. Dias, M. Fatima Vaz, J.Cruz Fernandes, “Behavior of Open-Cell Cordierite Foams under Compression” *J. Eur. Ceram. Soc.* **26** [1-2] 179-186 (2006).

40. K. Li, X.L. Gao, and G. Subhash, “Effects of Cell Shape and Cell Wall Thickness Variations on the Elastic Properties of Two-Dimensional Cellular Solids”, *Int. J. Sol. and Struct.,* **42** [5-6] 1777-1795 (2005).

41. Morgan Technical Ceramics Piezoelectrics, Morgan Technical Ceramics, Bedford, OH. http://www.morganelectroceramic.com/piezomaterials/index.html

42. T. Ogawa, “Poling Field Dependence of Ferroelectric Properties in Barium Titanate Ceramics”, *Jpn. J. Appl. Phys.,* **40** 5630-5633 (2001).

BIOGRAPHICAL SKETCH

Laurel Wucherer was born in 1986, in Orlando, Florida. Both of her parents are CPAs and her sister, Devon, is currently a senior in high school. Since visiting the University of Florida (UF) in the spring of 2004, she became fascinated with material science after seeing the interesting research and facilities available. After starting her studies, Laurel wanted to experience the best of research and industry and the 3-2 program helped her achieve that by finishing her undergraduate and advanced studies simultaneously. In December she will be receiving her bachelor's and master's degrees in material science and engineering.

During that time, she joined Dr. Juan C. Nino's research group, where she became well acquainted with the life of a research scientist including the frustrations, triumphs and interesting work hours. In order to maintain her sanity, Laurel became very involved in many extracurricular activities including a sorority, tennis club and dance company. These activities offered her a creative outlet and the opportunity to continue hobbies she enjoyed growing up. Laurel has thoroughly enjoyed her time at UF and would not have preferred any other university for her college career. After graduation, she will begin her professional career as a materials engineer at the Walt Disney Company in Orlando, Florida.